A MIS 9/ MIS 8 speleothem record of hydrological variability from Macedonia (F.Y.R.O.M.)

Eleonora Regattieri[1,2, 3,*], Giovanni Zanchetta[1,4], Ilaria Isola[4], Petra Bajo[5], Chiara Boschi[3], Natale Perchiazzi[1], Russell N. Drysdale[5,6], John C. Hellstrom[7], Alexander Francke[2,8], Bernd Wagner[2],

*corresponding author, eleonora.regattieri@unipi.it

[1]Dipartimento di Scienze della Terra, University of Pisa, Via S. Maria 53, 56126, Pisa Italy

[2]Institute of Geology and Mineralogy, University of Cologne, Zülpicher Str. 49a, 50674, Cologne, Germany

[3]Istituto di Geoscienze e Georisorse IGG-CNR, Via Moruzzi 1, 56126, Pisa, Italy

[4]Istituto Nazionale di Geofisica e Vulcanologia INGV, Via della Faggiola 32, 56126, Pisa Italy

[5]School of Geography, University of Melbourne, Victoria 3010, Australia

[6]EDYTEM, UMR CNRS 5204, Université de Savoie-Mont Blanc, 73376 Le Bourget du Lac cedex, France

[7]School of Earth Sciences, University of Melbourne, Victoria 3010 Australia

[8]School of Earth and Environmental Science, University of Wollongong, NSW 2522, Australia

Abstract

The period corresponding to Marine Isotope Stages 9 (MIS 9) offers the opportunity to study orbital and sub-orbital scale climate variability under boundary conditions different from those of better studied intervals such as the Holocene and the Last Interglacial. Yet, it is poorly represented in independently-dated continental archives around the Mediterranean Region. Here, we present a speleothem stable isotope record ($\delta^{18}O$ and $\delta^{13}C$) from the Former Yugoslavian Republic of Macedonia (F.Y.R.O.M., southern Balkans), which consists of two periods of growth broadly covering the ca. 332 to 292 ka and the ca. 264 to 248 ka intervals (MIS 9e-b and late MIS 8). We interpret the speleothem $\delta^{18}O$ as mostly related to regional hydrology, with variations that can be interpreted as due to changes in rainfall amount, with higher/lower values associated to drier/wetter condition. This interpretation is corroborated by a change in mineralogical composition between aragonite and calcite at ca. 328 ka, which marks increasing precipitation at the onset of MIS 9 and occurs within a trend of decreasing $\delta^{18}O$

values. Also the comparison with the multiproxy climate record available from the nearby Lake Ohrid seems to support the proposed interpretation. The MIS 9e interglacial appears to be characterized by wettest conditions between ca. 326 and 321 ka, i.e. lasting ca. five kyr. Decreasing precipitation and enhanced millennial scale variability matches the glacial inception (MIS9 d to b), with drier events at ca. 319 ka (ca. 2 kyr long) and 310 ka (ca. 1 kyr long), and a major rainfall reduction between 306 and 298 ka. The latter is followed by a prominent wetter period between 298 and 295 ka, for which carbon data values suggest high infiltration rate. Rainfall decreases again after 295 ka, and remain low until the growth interruption at ca. 292 ka. Resumption of the growth and progressive soil development, expressed by the carbon isotope record, occurred during the late part of MIS 8. Despite the rather high temporal uncertainty (average 6 ka), the speleothem hydrological record complements the environmental information provided by the Lake Ohrid record and also fits well to the framework of regional and extra-regional variability, showing similarities with pollen records from southern and western Europe, both at orbital and at sub-orbital time scale.

Key words: speleothem; southern Balkans; MIS9; millennial-scale variability

1-Introduction

Past interglacial periods can be seen as a series of natural experiments characterized by different boundary conditions (e.g. seasonal and latitudinal distribution of insolation, atmospheric greenhouse gas concentrations, extent of continental ice sheets), with different consequent effects on the character of climate change (Tzedakis et al., 2009). The Marine isotope stage (MIS) 9 spans the 335-280 ka period (Railsback et al., 2015) and is a valuable complement to the better-studied interglacial intervals such as the Holocene and MIS 5e. It has high obliquity and is characterized by strong positive insolation anomalies centered over the poles in both summer hemispheres during substage 9e (Berger, 1979). Based on the caloric summer half-year insolation, the early part of MIS 9 is the closest analog to the late Holocene throughout the last 450 ka (Ruddimann, 2007). MIS 9e has also the highest atmospheric CO_2 concentration of the preindustrial period (nearly 300 ppm, Bazin et al., 2013). Conversely, in the latter stages of MIS 9, following the peak interglacial, summer insolation at high latitudes was not particularly strong and CO_2 concentration decreased gradually. Thus, MIS 9 offers the opportunity to study interglacial climate evolution and sub-orbital scale variability under boundary conditions very different from the present and from more recent interglacial periods. Also the regional expression of interglacial warmth during MIS 9e is diverse: it is one of the most prominent interglacial in Southern hemisphere records (Petit et al. 1999; Hodell et al. 2000; King and Howard 2000), but at high latitudes of the North Atlantic region it is characterized by contrasting records of Sea Surface Temperature (SST) variations, ranging from relatively cool in records from the Nordic Seas (Koç et al. 2001; Helmke and Bauch 2003), to mild interglacial conditions in the northeastern subpolar to mid-latitude Atlantic Ocean (McManus et al. 1999; Mokkedem and McManus, 2017; Kandiano et al. 2004; Kostygov et al. 2010; Rodrigues et al. 2011). At mid-latitudes, coupled marine and terrestrial pollen records from the Iberian margin (Desprat et al., 2009; Roucoux et al., 2006; Tzedakis et al., 2004) and pollen records from long continental sequences in central-southern Europe and in the Mediterranean (Tzedakis et al., 2003; Reille and de Beaulieu, 1995; Reille et al., 2000, Sadori et al., 2016a) have revealed significant vegetation changes during the MIS 9e ice volume minimum and increasing variability during the following glacial inception and the early part of the following glaciation (MIS9-8 transition), (Roucoux et al., 2006; Desprat et al., 2009; Fletcher et al., 2013, Tzedakis et al., 2004).

Speleothems are highly sensitive recorders of climate and environmental properties (e.g. McDermott et al., 2004; Fairchild and Baker, 2012; Lachniet et al., 2009) and can be accurately dated by means of U/Th and U/Pb methods (e.g. Richards and Dorale, 2003; Woodhead et al., 2006). Past speleothem research focusing on the Mediterranean region has provided valuable insights into regional climate history (e.g. Bar-Matthews et al., 1999, 2000, 2003; Drysdale et al., 2005, 2006, 2007, 2009; Fleitmann et al., 2009; Jex et al., 2011; Göktürk et al., 2011; Regattieri et al., 2014a, 2014b, 2016a; Zanchetta et al., 2007, 2014, 2016; Zhornyak et al., 2011). However, beyond the Last Interglacial, high-resolution speleothem records from the Mediterranean are scarce (Ayalon et al., 2002; Bard et al., 2002; Bar-Matthews et al., 2003; Drysdale et al., 2004). In this study, we investigate the stable isotope geochemistry, the mineralogy and the growth history of a stalagmite (OH2) covering the MIS9-MIS8 interval, that originates from a cave in the south-western part of the Former Yugoslavian Republic of Macedonia (F.Y.R.O.M., Fig. 1). The cave is located within the watershed of Lake Ohrid, from which a detailed multiproxy record of climate history is available for the last ca. 633 ka (see Wagner et al., 2017 and references therein). The comparison of the OH2 speleothem record with the local climatic framework provided by the lake record allows a better understanding of regional environmental/climatic drivers of speleothem stable isotope composition and of the progression of events from the interglacial MIS9e to the following glacial inception. We then compare our reconstruction to the wider climate history available from Mediterranean and North Atlantic archives, to unravel how regional environment change is linked to extra-regional climate variability at orbital and at millennial time scale.

2-Study site

2.1 Cave description

Stalagmite OH2 (Fig. 2) was collected already broken from an unsurveyed cave located on a slope in the hills ca.16 km to the North-East of Lake Ohrid (Fig. 1). The cave opens at ca. 1130 m above sea level (a.s.l.) and is developed in Triassic to Early Jurassic platform carbonates of the Korabi Zone (Robertson and Shallo, 2000; Kilias et al., 2001), which consist mainly of intensively folded limestones and local dolostone (Hoffmann et al., 2010). Specifically, the cave is developed mainly within dolomitic rocks (Fig. 1). The cave is now fossil, sub-horizontal, ca. 150 m long and mostly composed of narrow passages developed in vadose regime, and is partly to completely filled by abundant concretions. Reconnaissance dating of other stalagmites yielded Middle to Late Pleistocene ages (our unpublished data). Today, the catchment is covered by a relatively deep soil that sustains a well-developed forest of mesophilus and montane trees including deciduous oaks (*Quercus* spp) and beeches, hornbeams, hazels and maples (*Fagus sylvatica, Carpinus betulus, Corylus colurna and Acer obtusatum*; Matevski et al., 2011).

2.2 Local climate

The climate of the area is sub-Mediterranean with continental influences (Panagiotopoulos et al. 2013). Moisture availability is linked to the penetration of westerly storm tracks across southern Europe, and to Mediterranean cyclogenesis, both occurring predominantly during winter (Dünkeloh and Jacobeit, 2003; Ulbrich et al., 2012). The amount of winter precipitation is inversely correlated to the North Atlantic oscillation (NAO) index (Ulbrich et al., 2012) because during negative NAO phases westerly storm tracks are shifted southward and bring more humidity from the Atlantic to the Mediterranean region, and because negative NAO phases in turn enhanced local cyclogenesis (Ulbrich et al., 2012). Mediterranean cyclogenesis is influenced also by others large-scale atmospheric patterns: it shows a positive correlation with the strength of the Scandinavian Pattern (characterized by an anticyclonic anomaly over Fennoscandia and western Russia, and by a negative pressure anomalies around the Iberian Peninsula), (Xoplaki, 2002); and a negative correlation with the East Atlantic-West Russian pattern (a dipole with high pressure over Fennoscandia and low pressure north of the Caspian Sea), (Xoplaki, 2002).

The warm, dry summers are related to the expansion of the Azores High (Xoplaki et al., 2003). Summer conditions are influenced also by the Asian and the African monsoon systems, with a negative correlation between monsoon strength and Mediterranean summer rainfall (see Ulbrich et al., 2012 and references therein). Local meteorology is influenced by the site's proximity to the Adriatic Sea, the surrounding mountains, and the thermal capacity of Lake Ohrid itself (Watzin et al. 2002; Wagner et al., 2009; 2012; Panagiotopoulos et al., 2013). Mean July and January temperatures in the lowlands are 21 °C and 1 °C respectively, with a mean annual temperature of 11 °C (Popovska and Bonacci, 2007). The mean annual precipitation at the lake altitude is ca. 750 mm/yr, and increases with elevation, with a measured value of 1194 mm/yr at 975 m a.s.l. (Popovska and Bonacci, 2007). Higher precipitation occurs during winter, when snowfalls are frequent (Wagner et al., 2009).

The stable isotope composition of local precipitation water has an average d-excess of ca. 14‰ (Anovsky et al., 1991; Eftimi and Zoto, 1997), suggesting a component of meteoric water evaporated from the eastern Mediterranean (e.g. Dotsika et al., 2010). Rainfall $\delta^{18}O$ values in the Ohrid watershed range from ca. -10.2‰ and -8.2‰, with a mean value of -8.8‰, whereas precipitation δD values average -57‰ (Anovsky et al., 2000; Leng et al., 2010). $\delta^{18}O$ from springs around the lake range from −4.9‰ to −11.2‰ (including non-karstic springs). The range in spring/river $\delta^{18}O$ and δD overlaps with the calculated isotope composition of monthly precipitation (see Leng et al., 2010 for calculation), although most of the measured spring water isotope data concentrate in the lower isotope range. This suggest both that these springs are recharged at higher altitude and that they are supplied mainly by isotopically depleted winter rainfall and snowfall, given the seasonal distribution of precipitation in the region (Leng et al., 2010, 2013).

3- Material and methods

3.1- Sample description and subsampling

Stalagmite OH2 is 145 mm long and 105 mm wide at the base, with a pronounced conical shape (Fig. 2). It shows slight changes in the direction of the growth axis, perhaps due to earthquakes, which are common in the region (e.g. Hoffmann et al., 2010; Wagner et al., 2012). The basal section (145-132 mm depth from top, dft) of OH2 is mostly composed of aragonite. Above 132 mm dft OH2 is composed of calcite and shows several marked color changes (Fig. 2). The stalagmite was cut longitudinally and one of the halves was hand-polished and subsampled along the growth axis for stable isotope ($\delta^{13}C$ and $\delta^{18}O$) analyses. Subsampling was performed at 1-mm increments using a milling machine with a 1 mm-diameter drilling bit at the INGV laboratory of Pisa, producing 152 samples. For U/Th dating, 25 solid prisms of ca. 50 mg (ca. 2 mm wide along the lamina and 1 mm thick on growth axis) were taken from the calcite portion with a hand dental drill. In the aragonite portion of the stalagmite, due to the higher U content, 8 powder samples of ca. 15 mg were retrieved for the analyses. From the other half of OH2, on the face opposite the stable isotope subsampling, four overlapping thin sections were cut for mineralogical analyses. The thin sections were analyzed with a transmitted-light microscope (Zeiss Laboval 4 ausJena) and photographed with a digital camera (Canon EOS).

3.2 Stable isotope analyses

Stable isotope analyses were performed using a GasBench II (Thermo Scientific) coupled to a Delta XP Isotope Ratio Mass Spectrometer (Delta XP IRMS, Finnigan) at the Institute of Geosciences and Earth Resources of the Italian National Research Council (IGG-CNR) of Pisa (Italy). About 0.12 mg of $CaCO_3$ were dissolved in H_3PO_4 (100%) and reacted at 70°C for one hour. All the results were reported relative to the V-PDB international standard.

Sample results were corrected using the international standard NBS-18 and a set of three internal standards, previously calibrated using the international standards NBS-18 and NBS-19 and by inter-laboratory comparisons. Analytical uncertainties (1SD) are 0.10‰ and 0.15‰ for $\delta^{13}C$ and $\delta^{18}O$ respectively.

3.3 U/Th dating and age modelling

The U/Th dating was performed following the method of Hellstrom (2003) at the University of Melbourne (Australia). Briefly, samples were dissolved and a mixed ^{236}U-^{233}U-^{229}Th spike was added prior to removal of the carbonate matrix with ion-exchange resin. The purified U and Th fraction diluted in nitric acid was introduced to a multi-collector inductively coupled plasma mass spectrometer (MC-ICPMS, Nu-Instruments Plasma). The $^{230}Th/^{238}U$ and $^{234}U/^{238}U$ activity ratios were calculated from the measured atomic ratios using an internally standardized parallel ion-counter procedure and calibrated against the HU-1 secular equilibrium standard. Correction for detrital Th content was applied using initial activity ratios of detrital thorium ($^{230}Th/^{232}Th$)i of 1.5 ± 1.5. Two separate depth-age models (Fig. 3) were constructed using a Bayesian Monte Carlo approach (Scholz et al., 2012). One model comprises the basal aragonite and the lower calcite intervals and the other the calcite section at the top of the stalagmite. Age models were constructed including stratigraphical constrain following the method described in Hellstrom (2006).

3.4 Mineralogical analyses

XRD powder diffraction measurements were carried out on three samples of the basal aragonitic interval at the XRD1 beamline (Lausi et al., 2015) at the Elettra synchrotron facility, Basovizza, Trieste, Italy. The analyzed samples were gently hand milled in an agate mortar under acetone. The powders were transferred to 0.7 mm Lindemann borosilicate capillaries. XRD powder patterns were collected using a monochromatic wavelength of 0.5903 Å (21.00 keV) and 500 × 500 μm² spot size, using a Dectris Pilatus 2M hybrid-pixel area detector (DECTRIS Ltd., Baden-Daettwil, Switzerland). A preliminary calibration of the hardware setup was performed through the analysis of the powder pattern obtained using a 0.1 mm capillary LaB6 standard reference powder (NIST 660a) sample. Collected bi-dimensional powder patterns were subsequently integrated through the FIT2D (Hammersley, 1997) software, and the resulting 1-D patterns are reported in Figs. S1, S2, S3. A quantitative Rietveld analysis was performed through the TOPAS-Academic program (Coelho, 2004). A preliminary Pawley refinement (Pawley, 1981) was performed to get starting values for cell parameters and background, modeled with a 1/x function, effective to describe background intensity at low angles due to air scattering, and with a 12-term Chebyshev function. The effect of asymmetry, zero error and absorption were accounted for, and resulted quite limited. The instrumental contribution to the peak shape was modelled through a pseudo-Voigt function, by fitting the data of a sample of SRM 660a (LaB6) collected under the same experimental setup. Peak-shape broadening was modelled taking into account Gaussian crystallite size and microstrain contributions. The refined region for all samples was from 5-35° 2θ. Crystal structure models for calcite and aragonite were taken from Effenberger et al. (1981) and Ye et al. (2012) respectively. Only cell parameters were refined for the two phases, leaving unvaried atomic positional and displacement parameters. The Rietveld refinement (Rietveld, 1969) was led up to the satisfactory agreement factors reported in Table S1. Refined cell parameters for calcite (Table S2) are always close to literature values for pure calcite, pointing to a quite limited Mg content in all the samples (Table S3). Refined cell parameters for aragonite are shown in Table S4.

4- Results

4.1 Lithology and mineralogy

Petrographic investigation on thin sections, retrieved in continuous sections along the growth axis, shows that the basal 13 mm of OH2 are mostly composed of aragonite. Darker layers in the upper portion are probably due to organic material or clay (Fig. 4a). This interval shows typical aragonite ray crystals, with a width/length (W:L) ratio exceeding 6:1, an elongation along the *c*-axis and a uniform to patchy extinction (Fig. 4a). Specific calcite regions cannot be observed. However, detailed synchrotron mineralogical investigations of three samples within this section (Fig. 2) reveal a low amount of low-

Mg calcite (Table 1 and Table S3), suggesting a subtle, “cryptic” alteration in a sample apparently unaltered (Bajo et al., 2016). Aragonite-to-calcite transformation is indeed a common diagenetic process in speleothems and in aragonitic-biogenic carbonates (e.g. Gill et al., 1995; Zhang et al., 2014). The aragonite section is separated from the upper calcite portion by a rough surface clearly indicating a growth interruption (Fig. 4a). The calcite portion includes two intervals of continuous growth, which are separated by a hiatus at 24 mm dft (Fig. 4d-e). The calcite shows an elongated (W:L >6:1), compact columnar fabric (Fig. 4b-d). In the lower portion, crystals display mostly flat faces and are more elongated (crystal length of ca. 2 mm). They show a tendency to a radi-axial to feathered columnar fabric (Fig. 4b) with uniform to radi-axial extinctions, which are likely triggered by a high Mg content of the solution related to the dolomitic bedrock (Neuser and Richter, 2007; Frisia and Borsato, 2010) and by the slow growth rate. Above this, the crystals became progressively smaller (mean length of ca. 1 mm at the top of the section, Fig. 4d), less elongated and show more defects, such as lateral overgrowth (Fig. 4d).

4.2 Chronology

The six corrected U/Th ages obtained from the aragonitic portion of OH2 range from 330.50 ± 11.06 ka to 329.228 ± 11.93 ka. The 21 corrected U/Th ages of the lower calcite section of OH2 provided ages between 323.42 ± 18.46 ka and 292.05 ± 14.11 ka (Table 2). Four ages obtained in the upper calcite portion range from 263.11 ± 7.83 ka to 264.77 ± 5.28 ka. All the speleothem ages, here and after, are referred to b2k according to the reference standardized speleothem database (SISAL, Comas-Bru et al., 2017). Almost all ages are in stratigraphic order within the associated uncertainties. Only two ages were rejected as outliers (Table 2). As described above, mineralogical analyses show a small amount of aragonite to calcite transformation (Table 1). When neomorphism (i.e., the process of in-situ transformation of a mineral into a polymorph, Folk, 1965) occurs, most of the chemical properties can be re-set to the extent that they no longer fully represent the original conditions of deposition (Frisia et al., 2002; Zhang et al., 2014; Bajo et al., 2016). In particular, during aragonite-to-calcite transformation, U is commonly mobilized from the site of diagenesis, because recrystallization may involves a thin solution film in which U is easily mobilized (Domínguez-Villar et al., 2017), leading to an increase in the $^{230}Th/^{238}U$ isotopic ratio and resulting in U/Th ages which are older-than-true (Lachniet et al., 2012; Ortega et al., 2005; Bajo et al., 2016). This could severely compromise the accuracy of the U/Th chronology (Bajo et al., 2016). For OH2, petrographical and mineralogical observations show a limited occurrence of diagenetic alteration (more than 90% of aragonite preserved, see section 4.1). Moreover, the ages obtained from the aragonite section fit well with those of the calcite section above (Fig. 3). On the one hand, this suggests that the growth interruption between the aragonite and the calcite did not represent a significant time interval (i.e. it is within the associated uncertainty of the bounding ages). Moreover, it suggests that diagenesis does not significantly bias the accuracy of the U/Th chronology in the aragonite portion, otherwise ages for the aragonite portion would appear older (Lachniet et al., 2012; Ortega et al., 2005; Bajo et al., 2016). These considerations allow us to establish a continuous age-depth model for the aragonite-lower calcite section of OH2 between 151 and 23 mm dft, ranging from 332.08 ± 9.41 ka to 292.16 ± 6.00 ka (Fig. 3). The age model obtained for the calcite portion above 23 mm dft covers the 264.40 ± 10.84 ka to 247.47 ± 7.58 ka period. Due to the high number of performed dating, the uncertainties associated to the modelled age are significantly reduced with respect to those associated to single age measurements (average ca. 8.3 kyr in the upper calcite section, ca. 5.2 kyr for the central calcite section and ca. 5.7 kyr for the aragonite section; 2σ uncertainty). The resulting temporal resolution of the stable isotope record is highly variable, ranging from more than 1 kyr to 40 yr (Fig. 5).

4.3. Stable isotopes

Stable isotope results plotted versus ages are shown in Fig. 5. In the basal aragonite interval (Fig. 2) stable isotope values display maximum values (average -7.0 ‰ and -8.0 ‰ for oxygen and carbon respectively), with strongly decreasing values slightly before the end of the interval, from ca. 331 ± 6 ka to 328 ± 5 ka. $\delta^{18}O$ values in the calcite portion of OH2 range from -7.67‰ to -9.57‰. The interval of lowest values (averaging ca. -9.0‰) occurs between ca. 326 ± 6 ka and 321 ± 8 ka. After ca. 321 ka, values increase abruptly until 318 ± 8 ka, and decrease slightly subsequentely. A well-marked event of increasing $\delta^{18}O$, 1 kyr lasting, is apparent at ca. 310 ± 5 ka. At 306 ± 6 ka values increase abruptly and remain higher until 298 ± 5 ka (Fig. 5). From ca. 298 to 295 ± 5 ka values abruptly decrease again, then rapidly increase and remain around -7.8‰ until the end of the interval at 292 ± 8 ka. Above the hiatus, from 264 ± 8 ka to the top of the record at 248 ± 8 ka, $\delta^{18}O$ values are relatively stable between -8.0‰ and -8.6‰.

The calcite $\delta^{13}C$ values of OH2 range from -6.87‰ to -10.20‰ (Fig. 5). Rather stable values around ca. -10‰, with only minor oscillations of ca. 0.5-0.7‰, occur throughout the 328 - 292 ka period of growth, except for an abrupt shift toward higher values (ca. -8.3‰) from 299 to 295 ka, when the $\delta^{18}O$ record shows a prominent negative peak (Fig. 5). After the hiatus, from 264 ka onward, $\delta^{13}C$ values are at their maximum, but rapidly decrease, reaching values close to the previous interval from ca. 256 ±8 ka to the top of the record at ca. 248 ka.

5 Discussion

5.1 The aragonite interval: paleoclimate implications and the stable isotope record

The presence of aragonite in stalagmites is usually ascribed to low drip rate (Frisia et al., 2002) often coupled with high drip-water Mg concentration related to prior calcite precipitation (Fairchild and Treble, 2009), and/or to incongruent dissolution and long water residence time in dolomitic bedrock (Piccini et al., 2008; Regattieri et al., 2014b), such as that hosting the OH2 cave. All these processes occur during dry conditions; therefore, the presence of cave aragonite is an indicator of paleo-aridity

(Frisia et al., 2002; McMillian et al., 2005; Wassenburg et al., 2012). The stable isotope geochemistry of aragonite speleothem has been less investigated for paleoclimatic purposes compared to calcite (Frisia et al., 2002; McMillian et al., 2005; Li et al., 2011), as the relationships between aragonite fabric and isotopic equilibrium conditions are less well known. However, the crystal ray habit observed in OH2 has been identified as likely precipitating close to isotopic equilibrium (Frisia et al., 2002; Frisia and Borsato, 2010). Laboratory and field studies have demonstrated that different isotope fractionation factors for calcite and aragonite precipitating in equilibrium from the same solution cause enrichment in both carbon and oxygen isotope composition in aragonite (e.g. Tarutani et al. 1969; Romanek et al., 1992; Frisia et al., 2002). In Clamouse Cave, France (Frisia et al., 2002), which has a temperature of 14.5°C, so close to MAT at the OH2 site, the $\delta^{18}O$ value at the tips of active stalagmites is 0.7 to 1.4‰ (average 1.0 ‰) heavier than stalagmite calcite formed from waters with similar oxygen isotope values (Frisia et al., 2002). Assuming deposition close to isotopic equilibrium, $\delta^{18}O$ aragonite values can thus be corrected (i.e. calibrated to calcite) applying the appropriate aragonite-calcite fractionation offset. However, the diagenetic transformation of aragonite into calcite has been shown to produce a variable $\delta^{18}O$ offset, which may prevent the simple translation of aragonite $\delta^{18}O$ values into the "primary" calcite range. For example, Zhang et al., (2014) reported a depletion of 0.85‰± 0.29‰ in $\delta^{18}O$ values in secondary calcite (containing 10% of aragonite relicts) with respect to primary aragonite from the same growth layer. In most environments, recrystallization occurs from the interaction of fluid solutions with aragonite crystals. This diagenetic process can occur under open or semi-closed geochemical conditions (Domínguez-Villar et al., 2017). Open conditions result from the formation of voids due to dissolution of primary aragonite crystals and subsequent cementation with calcite crystals (Martín-García et al., 2014). In this case, secondary calcite crystals record the composition of the fluid at the time of diagenesis and do not longer reflect the original fluid composition. Under semi-closed conditions, instead, recrystallization results from the nearly simultaneous aragonite dissolution and calcite precipitation through a solution film <1 mm thick; and the secondary calcite composition is partly inherited from the composition of the primary aragonite (Domínguez-Villar et al., 2017). For stalagmite OH2, petrographical observations (section 4.1) do not suggest large alteration by a significant water flux, because specific calcitic areas are not observed within the aragonite interval. Also, the amount of diagenetic calcite is rather low (average 7.5%, Table 1) ensuing that the bulk speleothem oxygen composition primarily reflect the original aragonite $\delta^{18}O$ values, as the amount of preserved aragonite is more than 90%. Thus, we can tentatively apply a first-order correction to the OH2 $\delta^{18}O_{aragonite}$ values (Fig. 5), to bring them in the range of the primary calcite. After subtracting 1.0 ‰ (mean value from field study, Frisia et al., 2002), most of the $\delta^{18}O$ values still remain considerably higher with respect to the calcite portion (Fig. 5) and the trend of strongly decreasing values observed at the end of the aragonite section continues in the basal calcite section.

The increase in $\delta^{13}C$ values predicted from the different enrichment factors for calcite and aragonite forming from the same waters is ca. 1.7‰, and is independent of temperature between 10° and 40°C (Morse and Mackenzie 1990; Romanek et al., 1992). However, field measurements at Clamouse Cave show an increase from 2 to 3.4‰ in carbon isotope composition with respect to co-precipitating calcite, thus slightly higher than the predicted value, also for aragonite precipitating near isotopic equilibrium (Frisia et al., 2002). The unpredicted increase in $\delta^{13}C$ indicates that aragonite probably formed under slower, more constant, and more prolonged degassing conditions than calcite (Frisia et al., 2002). The complexity of phenomena that control ^{13}C-enrichment in speleothem aragonite precludes applying a simple translation of $\delta^{13}C$ data in the range of primary calcite, and prevents the discussion of their paleoclimatic meaning. Therefore, we will not discuss further the carbon record for the aragonite interval.

5.2. The $\delta^{18}O$ record and its paleoclimatic interpretation in the local environmental framework

The cave from which OH2 was retrieved was visited randomly several times since 2009, in different periods of the year and under different meteorological conditions. The cave always appeared hydrologically inactive, with no flowing and/or dripping water and no active speleothem growth. Thus, monitoring of modern drip and paired studies on modern calcite, normally recommended to test equilibrium deposition and the relationship between drip water and precipitation, was not possible. However, for OH2, deposition close to isotopic equilibrium can be inferred from the observed columnar fabric, which is thought to occur when speleothems are continuously wet, under relatively constant flow and from fluids at near-isotopic equilibrium conditions (Frisia et al., 2002; Frisia and Borsato, 2010, Frisia et al., 2015). The oxygen isotope composition of speleothems precipitating close to isotopic equilibrium depends on the isotopic composition of the drip water and on the cave air temperature (e.g. Lachniet et al., 2009). Isotopic fractionation factors between water and calcite has a temperature dependence of ca. -0.2‰ ± 0.03‰ $°C^{-1}$ between 5°C and 35°C (Kim and O'Neil, 1997), a value that has been recently update to -0.177‰$°C^{-1}$ specifically for speleothem calcite (Tremaine et al., 2011). In regards to relationships between precipitation and drip water, many studies from temperate to arid settings indicate that the $\delta^{18}O$ values of drip water appear to mostly represent, in relatively deep caves, the weighted mean annual $\delta^{18}O$ value of precipitation (Yonge et al., 1985; Fleitmann et al., 2004; Mattey et al., 2008; Piccini et al., 2008; Baneschi et al., 2011; Genty et al., 2014). In the absence of cave monitoring data and notwithstanding the limitation of this assumption, we can therefore assume that the same relationship holds for OH2 cave. However, probably in our case the recharge is likely mostly biased toward the winter season, due to the prevalence of winter precipitation in the Ohrid Region.

Factors driving the oxygen isotopic composition of the meteoric precipitation ($\delta^{18}O_p$) and thus that of the speleothems, are multiple and vary on a spatial and temporal basis (e.g. Dansgaard et al., 1964; Lachniet et al., 2009; Demeny et al., 2017; Drăgusin et al., 2014). In the central and western

Mediterranean, the $\delta^{18}O_p$ has a strong, empirical relationship with the amount of rainfall (ca.-2.0‰ per 100 mm/month) and a negligible dependence on temperature (ca. +0.3‰/°C, i.e.; close in magnitude but opposite in sign to the cave-temperature effect, Bard et al., 2002). Lower $\delta^{18}O_{calcite}$ values during wetter periods are commonly reported from speleothems and carbonatic lake sediments from the region (e.g. Bar-Matthews at al., 2000, 2003; Bard et al., 2002; Drysdale et al., 2004, 2007; Regattieri et al., 2012, 2014a, 2015; Roberts et al., 2008, Zanchetta et al., 2007b, 2012, 2016a, 2017a; Giaccio et al., 2015a, 2015b). This general relationship has been also supported by multiproxy investigations on both kinds of deposits (Drysdale et al., 2006, 2009; Regattieri et al., 2016a, 2016b, 2017; Sadori et al., 2016b). In central and northern Europe, the $\delta^{18}O_p$ is strongly positively related to condensation temperature (+0.58‰ /°C, Rozansky et al., 1993), whereas the amount effect is negligible. This temperature dependence is reflected in the $\delta^{18}O$ of calcite from speleothems and lakes, which usually show lower values during colder periods and higher values during warmer periods (e.g. Mangini et al., 2005; Boch et al., 2011; Hauselmann et al., 2015; Spötl and Mangini, 2003; Spötl et al., 2006). In addition to these two main driving factors, there is an overall influence of changes in the isotopic values of the source of the precipitation (i.e. the sea surface water, e.g. Grant et al., 2012; Marino et al., 2015). The Balkan Peninsula is part of the Mediterranean region, but it is also is affected by continental processes. Speleothem records from the region are scarce and mostly located along the Adriatic coastline (Suric, 2005; Rudzka, 2012; Chiarini et al., 2017) or in the more continental region, north of the Balkans, in Romania or Hungary (e.g. Onac et al., 2002; Onac and Lauritzen, 2006; Tămaş et al., 2010; Demeny et al., 2017). For the F.Y.R.O.M. specifically, no other speleothem records are available to our knowledge, and the main drivers of $\delta^{18}O$ composition of speleothem calcite are not defined yet. If we hypothesize that, as for the Mediterranean, the $\delta^{18}O$ is mostly related to the amount effect, with lower values indicating wetter periods, the higher values and the decreasing trend observed in the calcite-calibrated $\delta^{18}O$ record of the aragonite interval are in good agreement with the large hydrological shift (from drier to wetter conditions) reflected by the change in speleothem mineralogy at ca. 328 ka. Following this hypothesis, the general pattern of OH2 $\delta^{18}O$ record shows significant similarities with paleoclimate proxies from the Lake Ohrid throughout the observed period (Fig. 5), supporting the interpretation of speleothem $\delta^{18}O$ as a hydrological proxy. The shift in isotope composition and mineralogy indeed corresponds to the abrupt rise in arboreal pollen (AP-*Pinus*) percentage (Sadori et al., 2016a) and in total inorganic carbon (TIC) content (Francke et al., 2016) related to the MIS10-MIS9 transition (Fig. 5). Increase in AP indicates rising temperature and precipitation (Sadori et al., 2016a). Increase in TIC content of lake sediment implies high photosynthesis-induced precipitation of endogenic calcite, promoted by rising spring and summer temperatures (Francke et al., 2016). Moreover, the TIC content is also related to HCO_3^- and Ca^{2+} concentrations in the lake water, which depend on lake water evaporation, the intensity of chemical weathering of limestone in the catchment, the karst discharge volume and surface runoff (Vogel et al., 2010; Francke et al., 2016). These parameters are all related to the amount of precipitation, mostly occurring during winter, with enhanced ion supply through soil/epikarst dissolution processes and high soil CO_2 activity during increased rainfall. This dependence of TIC content to precipitation amount may explain the similarity to the OH2 $\delta^{18}O$ hydrological record. Between ca. 328 and 321 ka, lowest isotopic values of OH2 record are consistent with highest TIC and AP content in the lake record, within the associated uncertainties of both records (the mean 2σ uncertainties of the lake record, whose age model is based on tephrochronology and refined by tuning to local insolation, in this interval is ca. 2 kyr, Francke et al., 2016). Thus, both the speleothem and the lake records agree in showing high precipitation during this period. Within this interval, slightly reduced precipitation (increasing speleothem $\delta^{18}O$) is apparent at ca. 323 ka (Fig. 5). A sudden increase in $\delta^{18}O$ values at ca. 321 ka, indicating rainfall reduction, is followed by increased variability at multi-centennial scale until ca. 313 ka. In the lake record, this period is marked by a pronounced minimum in TIC and AP and a significant maximum in $\delta^{18}O$ values centered around 320 ka (Fig. 5). Slightly higher precipitation is apparent between 312 and 306 ka and is marked by lower $\delta^{18}O$ values of lake and speleothem calcite and higher AP and TIC, although all the proxies suggest that this interval is slightly drier than the previous interglacial peak (Fig. 5). In the stalagmite record, as well as in the lake TIC and AP record, this interval is interrupted by a sharp, 2.5-kyr-long drier event centered at ca. 310 ka (Fig. 5). From 306 ka speleothem $\delta^{18}O$ shows that precipitation decreases abruptly and remains low until ca. 297 ka, although with a brief wetter reversal centered at ca. 299 ka. A concomitant depressed temperature is suggested by a drop in endogenic calcite deposition and in AP content of lake sediments (Fig. 5). The break-down of calcite-precipitation preservation and the presence of siderite in the lake sediments suggest a glacial-like climate state persisting throughout much of this phase (Francke et al., 2016; Lacey et al., 2016). However, the continuous growth of OH2 in this period suggests temperatures above 0°C. After 297 ka, a stepwise abrupt decrease in speleothem $\delta^{18}O$ indicates enhanced precipitation. This wetter period matches, for shape and length, a spike in AP content, although TIC content does not show a similar increase. A drastic reduction of precipitation characterizes the period between 295 ka and the end of the section at ca. 292 ka. Resumption of speleothem growth after ca. 264 ka is marked in the lake record by slight increase in AP percentages (Fig. 5), but not in TIC, which suggests that relatively cold and dry conditions persisted.

5.3 The $\delta^{13}C$ record and its paleoclimatic interpretation

In temperate settings, increasing $\delta^{13}C$ values in speleothems are related to a more significant contribution of ^{13}C-enriched CO_2 from bedrock dissolution and/or to a decrease in soil-CO_2 productivity due to a reduction in rainfall and/or cooler climate (e.g. Genty et al., 2001). Reduction in recharge can also produce degassing along the fracture paths and longer rock-water interaction time, both resulting in higher $\delta^{13}C$ of drip water and speleothem (Baker et al., 1997; Fairchild et al., 2006).

Commonly, when oxygen is interpreted in hydrological terms, as in our case, a positive correlation is observed between $\delta^{13}C$ and $\delta^{18}O$ values, with a reduction of soil biological activity (higher $\delta^{13}C$) paired to a reduction in precipitation (higher $\delta^{18}O$). In the OH2 stalagmite, the $\delta^{13}C$ record is more stable with respect to $\delta^{18}O$ and characterized by relatively low values (Fig. 5), which indicates a strong contribution of organic CO_2 from the soil both during the interglacial and during the following glacial inception. It suggests that the soil above the cave was relatively well developed during the whole period, enough to buffer the effect of precipitation changes recorded by the oxygen isotope record. Accordingly, the pollen record from the nearby Lake Ohrid (Sadori et al., 2016a) indicates a significant percentage of trees in the lake catchment also during part of the MIS10 and MIS8. However, it is worth noting that, although subdued, the variability observed in the $\delta^{13}C$ record during the period from ca. 330 to 297 ka resembles that observed in the $\delta^{18}O$ record (Fig. 5), suggesting a modulation of soil productivity related to rainfall fluctuations. The combination between lower $\delta^{18}O$ (intended as a hydrological proxy) and higher $\delta^{13}C$ values is reported more rarely. In periods when the soil–water residence time is relatively short (i.e. enhanced rainfall and very high infiltration rate), complete isotopic equilibration may not occur between soil CO_2 and the percolating H_2O, and the infiltrating water may retain a component of isotopically heavier atmospheric CO_2 in solution (Bar-Matthews et al., 2000; McDermott, 2004). Alternatively, high $\delta^{13}C$ paired with low $\delta^{18}O$ can be the result of enhanced weathering of the host rock, potentially related to reaction of oxygenated water with sulphide minerals. This process is common in dolomitic bedrock and tends to produce sulphuric acid which, by promoting dissolution, will enhance the host rock $\delta^{13}C$ contribution (Bajo et al., 2017), and the supply of more ^{13}C-enriched carbon, due to high water flux. Similar processes may explain the positive $\delta^{13}C$ values paired with the negative $\delta^{18}O$ values between 297 and 295 ka and likely indicate a prominent increase in precipitation (Fig. 5). After the hiatus, from 264 ka, rapidly decreasing $\delta^{13}C$ values may represent the progressive reestablishment of soil and vegetation in the catchment following the maximum of glacial MIS8 (Fig. 5). This, and the presence of the preceding hiatus, may suggest temperature below 0°C and/or that the catchment was ice-covered during the MIS8 maximum. In the Balkans, glaciations may have taken place during MIS8, although deposits have not been preserved due to later glaciations being more extensive (Hughes et al., 2006). Indeed, extensive evidences of glaciation in the area were reported by Ribolini et al., (2011, 2017).

5.4 The Ohrid record in a Mediterranean-North Atlantic context

At orbital scale the OH2 record broadly matches the latest part of Termination IV and the isotopic sub-stages of MIS 9e-b and 8b of the global stacked benthic record LR04 (Lisiecki and Raymo, 2005). However, marine-pollen records covering MIS9 have shown that the onset and the demise of benthic and terrestrial stadials and interstadials have a variable phasing, and that their length can significantly differ (Tzedakis et al., 2004; Roucoux et al., 2006; Desprat et al., 2009), as already observed for MIS5 (Shackleton et al., 2003). In the following discussion we will refer to the terrestrial counterparts of the marine stages as defined by Tzedakis et al. (2004) on the basis of vegetation changes from core MD01-2443 (Fig. 6), retrieved in the southern Portuguese margin (Fig. 1). The distinct mineralogical change and strongly decreasing $\delta^{18}O$ values indicated in the OH2 record at ca. 328 ka represent increasing precipitation related to the MIS10-MIS 9 transition. Wettest conditions following this shift since 326 ka prevail only briefly. The sudden reduction in precipitation apparent at ca. 321 ka indeed marks the end of the interglacial optimum. The early end of the interglacial optimum observed in our record may correspond to a regional event of forest decline observed from Greece to Spain (Tzedakis et al., 2004, 2006; Desprat et al., 2009) and in the MD01-2443 record (Fig. 6; Tzedakis et al., 2004; Roucoux et al., 2006), where the length of terrestrial climate optimum of the 9e interglacial is similar (ca. four ka, Tzedakis et al., 2004). Also the speleothem $\delta^{18}O$ record from Corchia Cave (Central Italy; Drysdale et al., 2004), interpreted in turn as related to the amount effect, shows only a short interglacial precipitation maximum followed by a progressive trend of aridification and increased variability, which however has a different pattern compared to our record. Interestingly, at the same time SST from the Iberian margin shows only a moderate decline, which may indicate a partial land-sea decoupling during the interglacial (Fig. 6; Tzedakis et al., 2004). Instead, an early end of peak interglacial conditions is reported in a recent SST record from the Gulf of Lions covering the last four glacial/interglacial cycles (Cortina et al., 2015; Fig. 6). In this case, present and past SST changes are principally driven by variations in the intensity of northwesterly winds (the Mistral and Tramontana), blowing through the Pyrenees, the Massif Central, and the Alps (Cortina et al., 2011, 2013, 2015; Pinardi and Masetti, 2000). The early demise of peak interglacial conditions observed in this record (with respect to southern SST records) have been addressed as related to atmospheric patterns driven by high-latitude dynamics, like southward shifts of the atmospheric polar front and related persistent invasions of Arctic air masses (Cortina et al., 2015). The similarity observed with our record may suggest that during periods of reduced ice volume and strong MOC, atmospheric dynamics also became more influential on Mediterranean continental hydrology. Unstable hydrological conditions and slightly reduced precipitation for the 321-313 ka period mirror the stadial of MIS9d. On the Iberian margin, this interval was characterized by a less arid and warmer climate compared to the subsequent stadial MIS9b (Roucoux et al., 2006; Desprat et al., 2009), although punctuated by several millennial-scale events of forest reduction and/or SST cooling (Roucoux et al., 2006; Desprat et al., 2009). Despite the relative age uncertainties associated with both records prevent a detailed correlation, the general pattern observed in our record and in the pollen records from the Iberian margin is very similar (Fig. 6). The subsequent period, from 313 to 306 ka, corresponds to interstadial MIS9c and shows a generally wetter climate marked by an abrupt event of reduced precipitation at ca. 310 ka. On the Portuguese margin, this interstadial appears characterized by two warm intervals with higher SST and forest expansions interrupted by a cooler/drier phase in between (Fig. 6; Roucoux et al., 2006; Desprat et al., 2009). This event corresponds to a prominent event of ice rafted debris (IRD) deposition in the subpolar North Atlantic (McManus et al., 1999). It also marks the overrun of the $\delta^{18}O$ benthic value of 3.5‰, considered by some as the critical threshold for ice volume triggering ice sheet instability, large iceberg discharge and disruption of Atlantic meridional overturning circulation (AMOC), with associated increase in the amplitude of sub-orbital SST reductions (McManus et al., 1999). A drastic reduction of arboreal vegetation is apparent within the MIS9c also in the high resolution pollen record from Tenaghi Philippon (TP, Greece, Fig. 6; Fletcher et al., 2013). In TP, increased variability at millennial time scales is observed during the early glacial (MIS9c-a) and was addressed as related to climate dynamics involving interhemispheric coupling via the bipolar see-saw (EPICA Community Members, 2006) and the rapid transmission of Atlantic climate variability into the Mediterranean region (Fletcher et al., 2013). In spite of the chronological mismatching, the general pattern of millennial-scale variability observed in our record resembles that of the TP pollen record (Fig. 6). This suggests that precipitation instability in the Ohrid region during the glacial inception can be likely linked to the reduction of northward oceanic heat transport associated with changes in North Atlantic circulation and European atmospheric gradients. The drastic precipitation decrease since 306 ka mirrors stadial conditions of MIS9b. On the Iberian margin, this interval corresponds to a pronounced tree population collapse and to the expansion of steppe vegetation, indicating dry and cold conditions related to a moderate and brief incursion of sub-polar water off the Iberian margin. In the TP record, this interval is characterized by cool conditions with fluctuating humidity (Fletcher et al., 2013). In particular, a well-expressed peak in arboreal vegetation during this stadial shows a very good match with the abrupt peak in precipitation apparent in our record between 297 and 295 ka (Fig. 6). After this peak, arboreal vegetation at TP decreases strongly and OH2 temporarily ceased deposition, thus the interstadial MIS9a is not represented in our record. The resumption of growth at ca. 264 ka suggests a wetter interval and warmer temperature leading to the progressive development of soil above the cave. This interval of climatic amelioration could correspond to the distinct climatic transition apparent during MIS 8 in pollen record from TP, where a re-expansion of arboreal populations and deepening of local water depth were observed (Fig. 6; Fletcher et al., 2013). Again, the short-term precipitation variability could resemble the small changes apparent in vegetation composition at TP, although detailed correlations are prevented by the associated uncertainties of both records. On a wider scale, North Atlantic and Mediterranean SST rose during this period and the Asian monsoon was re-invigorated (Jiang et al. 2010), suggesting a hemispheric intensification of the hydrological cycle (Fletcher et al., 2013). Our record ends at ca. 248 ka, because the very top part of the stalagmite is missing (Fig. 2).

6-Conclusions

The stalagmite (OH2) from F.Y.R.O.M. (Southern Balkans) consists of two intervals of growth covering the time periods between ca. 332 to 292 ka and ca. 264 to 248 ka, corresponding to the latter part of the MIS10 to 9 transition and to sub-stages 9e to 9b, and to the latter part of MIS8 respectively. We interpret the speleothem oxygen isotope variations as related largely to variations in rainfall amount, with decreasing/increasing values indicating wetter/drier conditions. This is supported by the speleothem mineralogy and by the similarity of the speleothem oxygen record with the multiproxy record from the nearby Lake Ohrid. The OH2 $\delta^{18}O$ record shows increasing precipitation related to the glacial/interglacial transition, which is also marked by a shift in speleothem mineralogy from aragonite (indicating drier conditions) to calcite (indicating wetter conditions) occurring at ca. 328 ka. From ca. 325 and 321 ka the record shows the highest rainfall associated to peak interglacial conditions of MIS9e. The length of the interglacial wettest period (ca. 6 ka) is similar to that observed in pollen and speleothem records from western and southern Europe (Tzedakis et al., 2004; Roucoux et al., 2006; Desprat et al., 2009; Drysdale et al., 2004) and in the SST record from the Gulf of Lions (Western Mediterranean, Cortina et al., 2015), and shorter with respect to SST records from the Iberian Margin (Tzedakis et al., 2004; Roucoux et al., 2006; Desprat et al., 2009; Martrat et al., 2007). This suggests a decoupling between North Atlantic conditions and Mediterranean continental hydrology during period of low ice volume and strong AMOC, with atmospheric dynamics becoming perhaps more influential. Unstable hydrological conditions and slightly reduced precipitation are apparent in the OH2 record for the 321-313 ka period and mirror stadial conditions of MIS 9d, which on the Iberian Margin appears similarly punctuated by several millennial-scale events of forest reduction and/or SST cooling. The subsequent period, from 313 to 306 ka, corresponds to MIS 9c and shows a generally wetter climate marked by an abrupt event of reduced precipitation at ca. 310 ka. The event is apparent also in pollen records from the Iberian Margin and from Southern Europe (Tzedakis et al., 2004; Roucoux et al., 2006; Desprat et al., 2009, Fletcher et al., 2013), and corresponds to a prominent event of IRD deposition in the subpolar North Atlantic (McManus et al., 1999). The occurrence of this event in our record suggests that precipitation instability in the Ohrid region during the glacial inception can be likely linked to the reduction of northward oceanic heat transport associated with changes in North Atlantic circulation and associated atmospheric patterns. Reduced precipitation and fluctuating humidity characterized the period from 306 ka to the growth interruption at ca. 292 ka. Within this interval, a strong anticorrelation between low $\delta^{18}O$ values and highest $\delta^{13}C$ values between 299 and 295 ka suggest high infiltration rate and low equilibration between atmospheric and soil CO_2 in combination with a maximum in precipitation. Resumption of growth occurs at ca. 264 ka and decreasing $\delta^{13}C$ values suggest progressive development of soil above the cave after the maximum of glacial MIS8. This latter interval of growth resembles a re-expansion of arboreal populations in southern Europe and matches North Atlantic and Mediterranean SST rose, as well as intensification of the Asian monsoon (Fletcher et al., 2013).

Overall, the OH2 record suggests that hydrological variability in Southern Balkans can be linked to regional and extra-regional climatic patterns both during interglacial and glacial inception intervals, when an indirect influence of North Atlantic oceanic conditions and Northern Hemisphere ice sheet dynamics can be recognized. Finally, the similarity observed between the multiproxy record from Lake Ohrid and the OH2 oxygen isotope record highlights the great potential of future speleothem studies in the region. Indeed, following the approach proposed by Zanchetta et al. (2016b), through the alignment of proxy time series from both archives, it may be possible to integrate the Lake chronology with independent, radiometric constraints provided by the speleothem chronology

Acknowledgments

This paper is the result of CCALMA (Climate from CAves and Lakes in Macedonia) working group, which paralleled the development of the SCOPSCO-ICDP project on Lake Ohrid. During the completion of this work, ER was supported by project SFB806 "Our way to Europe". This work was partly funded by the Australian Research Council Discovery Project DP160102969 and by "Fondi di Ateneo" of GZ. We thank the Galicica National Park (www.galicica.org.mk), the Skopije Speleological Team "Peoni", S. Trajanovski (Hydrobiological Institute, Ohrid), O. Avramoski (Galicica Park, Ohrid) and D. Georgiev for the logistical and friendly support during field work.

References

Anovski, T., Andonovski, B., Minčeva, B., 1991. Study of the hydrological relationship between lakes Ohrid and Prespa. In: Proceedings of an IAEA International Symposium, IAEA-SM-Vienna, 11–15 March 1991, 319, 62.

Ayalon, A., Bar-Matthews, M., Kaufman, A. 1999. Petrography, strontium, barium and uranium concentrations, and strontium and uranium isotope ratios in speleothems as palaeoclimatic proxies: Soreq Cave, Israel. The Holocene 9(6), 715-722.

Ayalon, A., Bar-Matthews, M., Kaufman, A., 2002. Climatic conditions during marine isotope stage 6 in the eastern Mediterranean region from the isotopic composition of speleothems of Soreq Cave, Israel. Geology 30, 303–306.

Bajo, P., Hellstrom, J., Frisia, S., Drysdale, R.N., Black, J., Woodhead, J., Borsato, A., Zanchetta, G., Wallace, M.W., Regattieri, E., Haese, R. 2015. “Cryptic" diagenesis and its implications for speleothem geochronologies. Quaternary Science Reviews 148, 17-28.

Bajo, P., Borsato, A., Drysdale, R., Hua, Q., Frisia, S., Zanchetta, G., Hellstrom, J.C., Woodhead, J. 2017. Stalagmite carbon isotopes and dead carbon proportion (DCP) in a near-closed-system situation: An interplay between sulphuric and carbonic acid dissolution. Geochimica et Cosmochimica Acta 210, 208-227.

Baker, A., Ito, E., Smart, P. L., McEwan, R. F. 1997. Elevated and variable values of 13C in speleothems in a British cave system. Chemical Geology 136(3-4), 263-270.

Baneschi, I., Piccini, L., Regattieri, E., Isola, I., Guidi, M., Lotti, L., Mantelli, F., Menichetti, M., Drysdale, R.N., Zanchetta, G. 2011. Hypogean microclimatology and hydrology of the 800-900 m.a.s.l. in the Monte Corchia Cave (Tuscany, Italy): preliminary considerations and implications for paleoclimatological studies- Acta Carsologica 40 (1), 175-187.

Bard, E., Delaygue, G., Rostek, F., Antonioli, F., Silenzi, S., Schrag, D.P. 2002. Hydrological conditions over the western Mediterranean basin during the deposition of the cold Sapropel 6 (ca. 175 kyr BP. Earth and Planetary Science Letters 202, 481–494.

Bar-Matthews, M., Ayalon, A., Kaufman, A.,Wasserburg, G.J. 1999. The Eastern Mediterranean paleoclimate as a reflection of regional events: Soreq Cave, Israel. Earth and Planetary Science Letters 166, 85–95.

Bar-Matthews, M., Ayalon, A., Kaufmann, A. 2000. Timing and hydrological conditions of sapropel events in the eastern Mediterranean, as evident from speleothems, Soreq Cave, Israel. Chemical Geology 169, 145–156.

Bar-Matthews, M., Ayalon, A., Gilmour, M., 2003. Sea–land oxygen isotopic relationships from planktonic foraminifera and speleothems in the Eastern Mediterranean region and their implication for paleorainfall during interglacial intervals. Geochimica et Cosmochimica Acta 67, 3181–3199.

Bazin, L., Landais, A., Lemieux-Dudon, B., Toyé Mahamadou Kele, H., Veres, D., Parrenin, F., ... & Loutre, M. F. (2013). An optimized multi-proxy, multi-site Antarctic ice and gas orbital chronology (AICC2012): 120-800 ka. Climate of the Past 9(4), 1715-1731.

Berger, A., Crucifix, M., Hodell, D. A., Mangili, C., McManus, J.F., Otto-Bliesner, B., Pol, K., Raynaud, D., Skinner, L.C., Tzedakis, P.C., Wolff, E.W., Yin, Q.Z., Abe-Ouchi, A., Barbante, C., Brovkin, V., Cacho, I., Capron, E., Ferretti, P., Ganopolski, A., Grimalt, J. O., Hönisch, B., Kawamura, K., Landais, A., Margari, V., Martrat, B., Masson-Delmotte, V., Mokeddem, Z., Parrenin, F., Prokopenko, A.A., Rashid, H., Schulz, M., Vazquez Riveiros, N. 2015. Interglacials of the last 800,000 years. Reviews of Geophysics 54, 162-219.

Boch, R., Cheng, H., Spötl, C., Edwards, R. L., Wang, X., Häuselmann, P. 2011. NALPS: a precisely dated European climate record 120–60 ka. Climate oft he Past 7, 1247-1259.

Borsato, A., Frisia, S., Miorandi, R. 2015. Carbon dioxide concentration in temperate climate caves and parent soils over an altitudinal gradient and its influence on speleothem growth and fabrics. Earth Surface Processes and Landforms 40(9), 1158-1170.

Cheng, H., Sinha, A., Verheyden, S., Nader, F. H., Li, X. L., Zhang, P. Z., Yin, J. J., Yi, L., Peng, Y. B., Rao, Z. G., Ning, Y. F., Edwards, R.L. 2015. The climate variability in northern Levant over the past 20,000 years. Geophysical Research Letters 42(20), 8641-8650.

Chiarini, V., Couchoud, I., Drysdale, R., Bajo, P., Milanolo, S., Frisia, S., Greig, A., Hellstrom, J.C., De Waele, J. 2017. Petrographical and geochemical changes in Bosnian stalagmites and their palaeo-environmental significance. International Journal of Speleology 46(1), 33.

Coelho, A. A. 2004. Topas-Academic. A Computer Programme for Rietveld Analysis

Comas-Bru, L., Deininger, M., Harrison, S., Bar-Matthews, M. 2017. SISAL: A community-driven initiative to create a global database of speleothem data for model evaluation. In EGU General Assembly Conference Abstracts (Vol. 19, p. 1487).

Cortina, A., Sierro, F. J., González-Mora, B., Asioli, A., Flores, J. A. 2011. Impact of climate and sea level changes on the ventilation of intermediate water and benthic foraminifer assemblages in the Gulf of Lions, off South France, during MIS 6 and 7. Palaeogeography, Palaeoclimatology, Palaeoecology 309(3), 215-228

Cortina, A., Sierro, F. J., Filippelli, G., Flores, J. A., Berné, S. 2013. Changes in planktic and benthic foraminifer assemblages in the Gulf of Lions, off south France: Response to climate and sea level change from MIS 6 to MIS 11. Geochemistry, Geophysics, Geosystems 14(4), 1258-1276.

Cortina, A., Sierro, F. J., Flores, J. A., Martrat, B., Grimalt, J. O. 2015. The response of SST to insolation and ice sheet variability from MIS 3 to MIS 11 in the northwestern Mediterranean Sea (Gulf of Lions). Geophysical Research Letters 42(23).

Dansgaard, W. (1964). Stable isotopes in precipitation. Tellus 16(4), 436-468.

Demény, A., Kern, Z., Czuppon, G., Németh, A., Leél-Őssy, S., Siklósy, Z., Haszpra, L. 2017. Stable isotope compositions of speleothems from the last interglacial–Spatial patterns of climate fluctuations in Europe. Quaternary Science Reviews 161, 68-80.

Desprat S, Goni MFS, McManus JF, Duprat J, Cortijo E 2009. Millennial-scale climatic variability between 340 000 and 270 000 years ago in SW Europe: evidence from a NW Iberian margin pollen sequence Climate Past 5, 53–72.

Domínguez-Villar, D., Krklec, K., Pelicon, P., Fairchild, I. J., Cheng, H., & Edwards, L. R. (2017). Geochemistry of speleothems affected by aragonite to calcite recrystallization–Potential inheritance from the precursor mineral. Geochimica et Cosmochimica Acta, 200, 310-329

Dotsika, E., Lykoudis, S., Poutoukis, D. 2010. Spatial distribution of the isotopic composition of precipitation and spring water in Greece. Global and Planetary Change 71(3), 141-149.

Drăguşin, V., Staubwasser, M., Hoffmann, D. L., Ersek, V., Onac, B. P., Vereş, D. 2014. Constraining Holocene hydrological changes in the Carpathian–Balkan region using speleothem $\delta^{18}O$ and pollen-based temperature reconstructions. Climate of the Past 10, 1363.

Drysdale, R.N., Zanchetta, G., Hellstrom, J.C., Fallick, A.E., Zhao, J.X., Isola, I., Bruschi, G., 2004. Palaeoclimatic implications of the growth history and stable isotope ($\delta^{18}O$ and $\delta^{13}C$) geochemistry of a Middle to Late Pleistocene stalagmite from central-western Italy. Earth and Planetary Science Letters 227, 215–229.

Drysdale, R.N., Zanchetta, G., Hellstrom, J.C., Fallick, A.E., Zhao, J.X., 2005. Stalagmite evidence for the onset of the Last Interglacial in southern Europe at 129+/−1 ka. Geophysical Research Letters 32, 1–4.

Drysdale, R.N., Zanchetta, G., Hellstrom, J.C., Maas, R., Fallick, A.E., Pickett, M., Cartwright, I., Piccini, L., 2006. Late Holocene drought responsible for the collapse of Old World civilizations is recorded in an Italian cave flowstone. Geology 34, 101–104.

Drysdale, R.N., Zanchetta, G., Hellstrom, J.C., Fallick, A.E., McDonald, J., Cartwright, I. 2007. Stalagmite evidence for the precise timing of North Atlantic cold events during the early last glacial. Geology 35, 77–80.

Drysdale, R.N., Zanchetta, G., Hellstrom, J.C., Fallick, A.E., Sanchez-Goni, M.F., Couchoud, I., McDonald, J., Maas, R., Lohmann, G., Isola, I. 2009. Evidence for obliquity forcing of glacial termination II. Science 325, 1527–1531.

Dünkeloh, A., Jacobeit, J. 2003. Circulation dynamics of Mediterranean precipitation variability 1948–98. International Journal of Climatology 23(15), 1843-1866.

Effenberger, H., Mereiter, K., & Zemann, J. 1981. Crystal structure refinements of magnesite, calcite, rhodochrosite, siderite, smithonite, and dolomite, with discussion of some aspects of the stereochemistry of calcite type carbonates. Zeitschrift für Kristallographie-Crystalline Materials 156(1-4), 233-244.

Eftimi, R., Zoto, J. 1997. Isotope study of the connection of Ohrid and Prespa lakes. In: International Symposium "Towards Integrated Conservation and Sustainable Development of Transboundary Macro and Micro Prespa Lakes", Korcha, Albania.

EPICA community members. 2006. One-to-one coupling of glacial climate variability in Greenland and Antarctica, Nature 444, 195–198

Fairchild, I. J., Smith, C. L., Baker, A., Fuller, L., Spötl, C., Mattey, D., McDermott, F. 2006. Modification and preservation of environmental signals in speleothems. Earth-Science Reviews 75(1), 105-153.

Fairchild, I.J, Baker, A. 2012. Speleothem Science- from Processes to Past Environments. Quaternary Geosciences Series. Wiley-Blakwell:Oxford.

Fairchild, I. J., Treble, P. C. 2009. Trace elements in speleothems as recorders of environmental change. Quaternary Science Reviews 28(5), 449-468.

Fletcher, W. J., Müller, U. C., Koutsodendris, A., Christanis, K., Pross, J. 2013. A centennial-scale record of vegetation and climate variability from 312 to 240 ka (Marine Isoto pe Stages 9c–a, 8 and 7e) from Tenaghi Philippon, NE Greece. Quaternary Science Reviews 78, 108-125.

Fleitmann, D., Burns, S. J., Neff, U., Mudelsee, M., Mangini, A., Matter, A. 2004. Palaeoclimatic interpretation of high-resolution oxygen isotope profiles derived from annually laminated speleothems from Southern Oman. Quaternary Science Reviews 23(7), 935-945.

Fleitmann, D., Cheng, H., Badertscher, S., Edwards, R.L., Mudelsee, M., Göktürk, O.M., Fankhauser, A.,Pickering, R.,Raible, C.C.,Matter, A.,Kramers, J.,Tuysuz, O. 2009. Timing and climatic impact of Greenland interstadials recorded in stalagmites from northern Turkey. Geophysical. Research Letters 36, L19707.

Francke, A., Wagner, B., Just, J., Leicher, N., Gromig, R., Baumgarten, H., Vogel, H., Lacey, J. H., Sadori, L., Wonik, T., Leng, M. J. Zanchetta, G., Sulpizio, R., Giaccio, B. 2016. Sedimentological processes and environmental variability at Lake Ohrid (Macedonia, Albania) between 637 ka and the present. Biogeosciences 13(4), 1179-1196.

Frisia, S., Borsato, A., Fairchild, I.J., McDermott, F., Selmo, E.M., 2002. Aragonitecalcite relationships in speleothems (Grotte de Clamouse, France): environment, fabrics, and carbonate geochemistry. Journal of Sedimentary Research 72, 687-696.

Frisia, S., Borsato, A. 2010. Karst. Carbonates in continental settings. Developments in sedimentology 61, 269-318.

Folk, L.R., 1965. Some aspects of recrystallization in ancient limestones. In: Pray, L.C., Murray, R.C. (Eds.), Dolomitization and Limestone Diagenesis, SEPM, Special Publication 13, 14-48.

Giaccio, B., Regattieri, E., Zanchetta, G., Nomade, S., Renne, P. R., Sprain, C. J., Drysdale, R.N., Tzedakis, P.C., Messina P., Scardia, G., Sposato, A., Bassinot, F. 2015a. Duration and dynamics of the best orbital analogue to the present interglacial. Geology 43(7), 603-606.

Giaccio B., Regattieri E., Zanchetta G., Wagner B., Galli P., Mannella G., Niespolo E., Peronace E., Renne P., Nomade S., Cavinato G.P., Messina P., Sposato A., Boschi C., Florindo F., Marra F., Sadori L. 2015b. A key continental archive for the last 2 Ma of climatic history in central Mediterranean area: a preliminary report on the Fucino deep-drilling project, central Italy. Scientific Drilling 3, 1–7.

Gill, I., Olson, J. J., Hubbard, D. K. 1995. Corals, paleotemperature records, and the aragonite-calcite transformation. Geology 23(4), 333-336.

Genty, D., Baker, A., Vokal, B. 2001. Intra-and inter-annual growth rate of modern stalagmites. Chemical Geology 176(1), 191-212.

Genty, D., Labuhn, I., Hoffmann, G., Danis, P. A., Mestre, O., Bourges, F., Orengo, P. 2014. Rainfall and cave water isotopic relationships in two South-France sites. Geochimica et Cosmochimica Acta 131, 323-343.

Göktürk, O.M., Fleitmann, D., Badertscher, S., Cheng, H., Edwards, R.L., Leuenberger, M., Fankhauser, A., Tüysüz, O., Kramers, J., 2011. Climate on the southern Black Sea coast during the Holocene: implications from the Sofular Cave record. Quaternary Science Reviews 30, 2433–2445.

Grant, K. M., Rohling, E. J., Bar-Matthews, M., Ayalon, A., Medina-Elizalde, M., Ramsey, C. B., Roberts, A. P. 2012. Rapid coupling between ice volume and polar temperature over the past 150,000 years. Nature 491(7426), 744-747.

Hendy C. H. 1971. The isotopic geochemistry of speleothems-I. The calculation of the effects of different modes of formation on the isotopic composition of speleothems and their applicability as palaeoclimatic indicators. Geochimica and Cosmochimica Acta 35, 801–824.

Hammersley, A. P. 1997. FIT2D: an introduction and overview. European Synchrotron Radiation Facility Internal Report ESRF97HA02T, 68.

Häuselmann, A.D., Fleitmann, D., Cheng, H., Tabersky, D., Günther, D., Edwards, R.L. 2015. Timing and nature of the penultimate deglaciation in a high alpine stalagmitefrom Switzerland. Quaternary Science Reviews 126, 264-275.

Hellstrom, J.C. 2003. Rapid and accurate U/Th dating using parallel ion-counting multicollector ICP-MS. Journal of Analytical Atomic Spectrometry 18, 1346–1351.

Hellstrom, J.C. 2006. U-Th dating of speleothems with high initial 230Th using stratigraphical constraint. Quaternary Geochronology 1, 289–295.

Helmke, J.P, Bauch, H.A. 2003 Comparison of glacial and interglacial conditions between the polar and subpolar North Atlantic region over the last five climatic cycles. Paleoceanography 18:1036. doi:10.1029/2002pa000794

Hodell, D. A., Charles, C. D., Ninnemann, U. S. 2000. Comparison of interglacial stages in the South Atlantic sector of the southern ocean for the past 450 kyr: implications for Marine Isotope Stage (MIS) 11. Global and Planetary Change 24(1), 7-26.

Hoffmann, N., Reicherter, K., Fernández-Steeger, T., Grützner, C. 2010. Evolution of ancient Lake Ohrid: a tectonic perspective, Biogeosciences 7, 3377–3386

Hughes, P.D., Gibbard, P.L., Woodward, J.C. 2006. Middle Pleistocene glacier behaviour in the Mediterranean: sedimentological evidence from the Pindus Mountains, Greece. Journal of Geological Society 163 (5), 857-867.

Jex, C. N., Baker, A., Eden, J. M., Eastwood, W. J., Fairchild, I. J., Leng, M. J., Sloane, H. J. 2011. A 500yr speleothem-derived reconstruction of late autumn–winter precipitation, northeast Turkey. Quaternary Research 75(3), 399-405.

Jiang, X., Kong, X., Wang, Y., Cheng, H., Wu, J., Chen, S.T. 2010. Orbital- and millennial-scale variability of the Asian monsoon during MIS8 from Sanbao Cave at Mount Shennongjia, central China. Chinese Science Bulletin 55, 1041-1046.

Kandiano E.S., Bauch H.A. 2003. Surface ocean temperatures in the north-east Atlantic during the last 500 000 years: evidence from foraminiferal census data. Terra Nova 15: 265–271.

Kilias, A., Tranos, M., Mountrakis, D., Shallo, M., Marto, A., Turku, I. 2001. Geometry and kinematics of deformation in the Albanian orogenic belt during the Tertiary. Journal of Geodynamics 31(2), 169-187.

King, A. L., Howard, W. R. 2000. Middle Pleistocene sea-surface temperature change in the southwest Pacific Ocean on orbital and suborbital time scales. Geology 28(7), 659-662.

Koç, N., Labeyrie, L., Manthé, S., Flower, B.P., Hodell, D.A., Aksu, A. 2001. The last occurrence of Proboscia curvirostris in the North Atlantic marine isotope stages 9–8. Marine Micropaleontology 41, 9–23.

Kostygov, S., Kandiano, E., Bauch, H. 2010. Reconstruction of deepwater conditions in the North Atlantic during MIS 9 based on benthic foraminiferal assemblages. Oceanology 50, 397–407.

Lachniet, M.S. 2009. Climatic and environmental controls on speleothem oxygen-isotope values. Quaternary Science Reviews 28, 412–432.

Lachniet, M.S., Bernal, J.P., Asmerom, Y., Polyak, V. 2012. Uranium loss and aragonite-calcite age discordance in a calcitized aragonite stalagmite. Quaternary Geochronology 14, 26-37

Lacey, J. H., Francke, A., Leng, M. J., Vane, C. H., Wagner, B. 2015. A high-resolution Late Glacial to Holocene record of environmental change in the Mediterranean from Lake Ohrid (Macedonia/Albania). International Journal of Earth Sciences 104(6), 1623-1638.

Lausi, A., Polentarutti, M., Onesti, S., Plaisier, J. R., Busetto, E., Bais, G., Pifferi, A. 2015. Status of the crystallography beamlines at Elettra. European Physical. Journal Plus 130, 1-8.

Leng, M. J., Baneschi, I., Zanchetta, G., Jex, C. N., Wagner, H., Vogel, H. 2010. Late Quaternary palaeoenvironmental reconstruction from Lakes Ohrid and Prespa (Macedonia/Albania border) using stable isotopes. Biogeosciences 7, 3109–3122,

Leng, M. J., Wagner, B., Boehm, A., Panagiotopoulos, K., Vane, C. H., Snelling, A., Haidon, C., Woodley, E., Vogel., H., Zanchetta, G., Baneschi, I. 2013. Understanding past climatic and hydrological variability in the Mediterranean from Lake Prespa sediment isotope and geochemical record over the Last Glacial cycle. Quaternary Science Reviews 66, 123-136.

Li, T. Y., Shen, C. C., Li, H. C., Li, J. Y., Chiang, H. W., Song, S. R., Wang, J. L. 2011. Oxygen and carbon isotopic systematics of aragonite speleothems and water in Furong Cave, Chongqing, China. Geochimica et Cosmochimica Acta75(15), 4140-4156.

Lisiecki, L. E., Raymo, M. E. 2005. A Pliocene-Pleistocene stack of 57 globally distributed benthic δ18O records. Paleoceanography 20(1).

Mangini, A., Spötl, C., Verdes, P. 2005. Reconstruction of temperature in the Central Alps during the past 2000 yr from a δ 18 O stalagmite record. Earth and Planetary Science Letters 235(3), 741-751.

Marino, G., Rohling, E. J., Rodríguez-Sanz, L., Grant, K. M., Heslop, D., Roberts, A. P., Yu, J. 2015. Bipolar seesaw control on last interglacial sea level. Nature 522(7555), 197-201.

Martín-García R., Alonso-Zarza A. M., Martín-Pérez A., Schröder-Ritzrau A. and Ludwig T. (2014) Relationship between colour and diagenesis in the aragonite-calcite speleothems in Basajau´n cave, Spain. Sedimentray Geology 312, 63–75.

Martrat, B., Grimalt, J. O., Shackleton, N. J., de Abreu, L., Hutterli, M. A., Stocker, T. F. 2007. Four climate cycles of recurring deep and surface water destabilizations on the Iberian margin. Science 317(5837), 502-507.

Matevski, V., Čarni, A, Avramovski, O., Juvan, N., Kostadinovski, M., Košir, P., Marinšek, A., Paušič, A., Šilc, U., 2011.Forest vegetation of the Galičica mountain range in Macedonia.Zalozba ZRC, ZRC SAZU, Ljubljana.

Mattey, D., Lowry, D., Duffet, J., Fisher, R., Hodge, E., Frisia, S. 2008. A 53 year seasonally resolved oxygen and carbon isotope record from a modern Gibraltar speleothem: reconstructed drip water and relationship to local precipitation. Earth and Planetary Science Letters 269(1), 80-95.

McDermott F. 2004. Palaeo-climate reconstruction from stable isotope variations in speleothems: a review. Quaternary Science Reviews 23, 901–918.

McManus, J.F, Oppo, D.W., Cullen, J.L. 1999. A 0.5-million-year record of millennial-scale climate variability in the north Atlantic. Science 283, 971–975.

McMillan, E. A., Fairchild, I. J., Frisia, S., Borsato, A., & McDermott, F. 2005. Annual trace element cycles in calcite–aragonite speleothems: evidence of drought in the western Mediterranean 1200–1100 yr BP. Journal of Quaternary Science 20(5), 423-433.

Mokeddem, Z., & McManus, J. F. 2017. Insights into North Atlantic deep water formation during the peak interglacial interval of Marine Isotope Stage 9 (MIS 9). Climate Dynamics 1-16.

Morse, J. W., Mackenzie, F. T. 1990. Geochemistry of sedimentary carbonates, 48. Elsevier.

Neuser, R. D., Richter, D. K. 2007. Non-marine radiaxial fibrous calcites—examples of speleothems proved by electron backscatter diffraction. Sedimentary Geology 194(3), 149-154.

Onac, B. P., Constantin, S., Lundberg, J., Lauritzen, S. E. 2002. Isotopic climate record in a Holocene stalagmite from Ursilor Cave (Romania). Journal of Quaternary Science 17(4), 319-327.

Onac, B. P., Lauritzen, S. E. 1996. The climate of the last 150,000 years recorded in speleothems: preliminary results from north-western Romania. Theoretical and Applied Karstology 9, 9.

Ortega, R., Maire, R., Deves, G., Quinif, Y. 2005. High-resolution mapping of uranium and other trace elements in recrystallized aragonite-calcite speleothems from caves in the Pyrenees (France): implication for U-series dating. Earth Planetary Science Letters 237, 911-923.

Pawley, G. S. 1981. Unit-cell refinement from powder diffraction scans. Journal of Applied Crystallography 14(6), 357-361.

Panagiotopoulos, K., Aufgebauer, A., Schäbitz, F., Wagner, B. 2013. Vegetation and climate history of the Lake Prespa region since the Lateglacial. Quaternary International 293, 157-169.

Petit, J. R., Jouzel, J., Raynaud, D., Barkov, N. I., Barnola, J. M., Basile, I., Delmotte, M. 1999. Climate and atmospheric history of the past 420,000 years from the Vostok ice core, Antarctica. Nature 399(6735), 429-436.

Piccini, L., Zanchetta G., Drysdale, R.N., Hellstrom, J.C., Isola, I., Fallick, A.E., Leone, G., Doveri, M., Mussi, M., Mantelli, M., Molli, G., Lotti, L., Roncioni, A., Regattieri, E., Meccheri, M., Vaselli, L. 2008. The environmental features of the Monte Corchia cave system (Apuan Alps, central Italy) and their effects on speleothem growth- International Journal of Speleology 37 (3), 153-172.

Pinardi, N., Masetti, E. 2000. Variability of the large scale general circulation of the Mediterranean Sea from observations and modelling: a review. Palaeogeography, Palaeoclimatology, Palaeoecology 158(3), 153-173.

Popovska, C., Bonacci, O. 2007. Basic data on the hydrology of Lakes Ohrid and Prespa. Hydrological Process 21, 658–664.

Railsback, L. B., Gibbard, P. L., Head, M. J., Voarintsoa, N. R. G., Toucanne, S. 2015. An optimized scheme of lettered marine isotope substages for the last 1.0 million years, and the climatostratigraphic nature of isotope stages and substages. Quaternary Science Reviews 111, 94-106.

Reille, M. and de Beaulieu, J.-L. 1995Long Pleistocene pollen records from the Praclaux Crater, South-Central France, Quaternary Research 44, 205–215.

Reille, M., de Beaulieu, J.-L., Svobodova, V., Andrieu-Ponel, V., and Goeury, C. 2000. Pollen analytical biostratigraphy of the last five climatic cycles from a long continental sequence from the Velay region (Massif Central, France). Journal of Quaternary Science 15, 665-685.

Regattieri, E., Isola, I., Zanchetta, G., Drysdale, R. N., Hellstrom, J. C., Baneschi, I. 2012. Stratigraphy, petrography and chronology of speleothem concretion at Tana Che Urla (Lucca, Italy): paleoclimatic implications. Geografia Fisica e Dinamica Quaternaria 35, 141-152.

Regattieri, E., Zanchetta, G., Drysdale, R.N., Isola, I., Hellstrom, J.C., Roncioni, A. 2014a. A continuous stable isotopic record from the Penultimate glacial maximum to the Last Interglacial (159 to 121 ka) from Tana Che Urla Cave (Apuan Alps, central Italy). Quaternary Research 82, 450–461.

Regattieri, E., Zanchetta, G., Drysdale, R.N, Isola, I., Hellstrom, J.C., Dallai, L. 2014b. Lateglacial to Holocene trace element record (Ba, Mg, Sr) from Corchia Cave (Apuan Alps, central Italy): paleoenvironmental implications. Journal of Quaternary Science 29(4), 381-392.

Regattieri, E., Giaccio, B., Zanchetta, G., Drysdale, R. N., Galli, P., Nomade, S., Peronace, E.,Wulf, S. 2015. Hydrological variability over the Apennines during the Early Last Glacial precession minimum, as revealed by a stable isotope record from Sulmona basin, Central Italy. Journal of Quaternary Science 30(1), 19-31

Regattieri, E., Zanchetta, G., Drysdale ,R.N., Woodhead, J.D.,Hellstrom, J.C., Giaccio, B., Isola, I., Greig, A., Baneschi I. 2016a. Environmental variability between the penultimate deglaciation and the mid Eemian: insights from Tana che Urla (central Italy) speleothem trace element record". Quaternary Science Reviews 152, 80-92.

Regattieri, E., Giaccio, B., Galli, P., Nomade, S., Peronace, E., Messina P., Sposato, A., Boschi, C., Gemelli, M. 2016b. A multi-proxy record of MIS 11-12 deglaciation and glacial MIS 12 instability from the Sulmona Basin (central Italy). Quaternary Science Reviews, 32, 129-145.

Regattieri, E., Giaccio, B., Zanchetta, G., Nomade, S., Francke, A., Vogel, H., Drysdale, R.N., Perchiazzi, N., Wagner, B., Gemelli, M., Mazzini, I., Boschi, C., Galli, P., Peronace, E. 2017. A Last Interglacial record of environmental changes from the Sulmona basin (Central Italy), Palaeogeography Palaeoclimatology Palaeoecology 472, 51-66.

Ribolini, A., Isola, I., Zanchetta, G., Bini, M., Sulpizio, R. 2011. Glacial features on the Galicica Mountains, Macedonia, Preliminary report. Geografia Fisica e Dinamica del Quaternario 34, 247-255.

Ribolini, A., Bini, M., Isola, I., Spagnolo, M., Zanchetta, G., Pellitero, R., Mechernich, S., Gromig, R., Dunai, T., Wagner, B., Milevski, I. 2017. An Oldest Dryas glacier expansion in the Pelister Mountain (Former Yugoslavian Republic of Macedonia) according to ^{10}Be cosmogenic dating. Journal of the Geological Society, in press, DOI: 10.1144/jgs2017-038

Richards, D.A., Dorale J.A. 2003. Uranium-series chronology and environmental applications of speleothems Reviews in Mineralogy & Geochemistry 52, 407–460.

Rietveld, H. 1969. A profile refinement method for nuclear and magnetic structures. Journal of applied Crystallography 2(2), 65-71.

Roberts, N., Jones, M.D., Benkaddour, A., Eastwood, W.J., Filippi, M.L., Frogley, M.R.,Lamb, H.F., Leng, M.J., Reed, J.M., Stein, M., Stevens, L., Valero-Garcés, B.,Zanchetta, G., 2008. Stable isotope records of Late Quaternary climate andhydrology from Mediterranean lakes: the ISOMED synthesis. QuaternaryScience Reviews 27, 2426-2441.

Robertson, A., Shallo, M. 2000. Mesozoic–Tertiary tectonic evolution of Albania in its regional Eastern Mediterranean context. Tectonophysics 316(3), 197-254.

Rodrigues, T., Voelker, A.H.L., Grimalt, J.O., Abrantes, F., Naughton, F. 2011. Iberian Margin sea surface temperature during MIS 15 to 9 (580–300 ka): glacial suborbital variability versus interglacial stability. Paleoceanography 26:PA1204. doi:10.1029/2010pa001927

Romanek, C. S., Grossman, E. L., Morse, J. W. 1992. Carbon isotopic fractionation in synthetic aragonite and calcite: effects of temperature and precipitation rate. Geochimica et Cosmochimica Acta 56(1), 419-430.

Roucoux, K.H., Tzedakis, P.C., de Abreu, L., Shackleton, N.J. 2006. Climate and vegetation changes 180,000 to 345,000 years ago recorded in a deep-sea core off Portugal. Earth and Planetary Science Letters 249, 307–325.

Rozanski, K., Araguás-Araguás, L., Gonfiantini, R. 1993. Isotopic patterns in modern global precipitation. Climate change in continental isotopic records, 1-36.

Ruddiman, W. F. 2007. The early anthropogenic hypothesis: Challenges and responses. Reviews of Geophysics 45(4).

Rudzka, D., McDermott, F., Surić, M. 2012. A late Holocene climate record in stalagmites from Modrič Cave (Croatia). Journal of Quaternary Science 27(6), 585-596.

Sadori, L., Koutsodendris, A., Masi, A., Bertini, A., Combourieu-Nebout, N., Francke, A. Peyron, O. 2016a. Pollen-based paleoenvironmental and paleoclimatic change at Lake Ohrid (SE Europe) during the past 500 ka. Biogeosciences 13, 1423–1437

Sadori, L., Giraudi, C., Masi, A., Magny, M., Ortu, E., Zanchetta, G., Izdebski, A. 2016b. Climate, environment and society in southern Italy during the last 2000 years. A review of the environmental, historical and archaeological evidence. Quaternary Science Reviews 136, 173-188.

Scholz, D., Hoffmann, D. L., Hellstrom, J., Ramsey, C. B. 2012. A comparison of different methods for speleothem age modelling. Quaternary Geochronology, 14, 94-104.

Spötl, C., Mangini, A. 2002. Stalagmite from the Austrian Alps reveals Dansgaard–Oeschger events during isotope stage 3: Implications for the absolute chronology of Greenland ice cores. Earth and Planetary Science Letters 203(1), 507-518.

Spötl, C., Mangini, A., Richards, D. A. 2006. Chronology and paleoenvironment of Marine Isotope Stage 3 from two high-elevation speleothems, Austrian Alps. Quaternary Science Reviews 25(9), 1127-1136.

Shackleton, N. J., Sánchez-Goñi, M. F., Pailler, D., Lancelot, Y. 2003. Marine isotope substage 5e and the Eemian interglacial. Global and Planetary Change 36(3), 151-155.

Surić, M., Horvatinčić, N., Suckow, A., Juračić, M., Barešić, J. 2005. Isotope records in submarine speleothems from the Adriatic coast, Croatia. Bulletin de la Société géologique de France,176(4), 363-372.

Tarutani, T., Clayton, R. N., Mayeda, T. K. 1969. The effect of polymorphism and magnesium substitution on oxygen isotope fractionation between calcium carbonate and water. Geochimica et Cosmochimica Acta 33(8), 987-996.

Tămaş, T., Onac, B. P., Bojar, A. V. 2010. Lateglacial-Middle Holocene stable isotope records in two coeval stalagmites from the Bihor Mountains, NW Romania. Geological Quarterly 49(2), 185-194.

Tremaine, D. M., Froelich, P. N., Wang, Y. 2011. Speleothem calcite farmed in situ: modern calibration of δ 18 O and δ 13 C paleoclimate proxies in a continuously-monitored natural cave system. Geochimica et Cosmochimica Acta 75(17), 4929-4950.

Tzedakis, P. C., McManus, J. F., Hooghiemstra, H., Oppo, D. W., Wijmstra, T. A. 2003. Comparison of changes in vegetation in northeast Greece with records of climate variability on orbital and suborbital frequencies over the last 450 000 years. Earth and Planetary Science Letters 212(1), 197-212.

Tzedakis, P.C., Roucoux, K.H., de Abreu, L., Shackleton, N.J. 2004. The duration of forest stages in southern Europe and interglacial climate variability. Science 306, 2231–2235.

Tzedakis, P. C., Raynaud, D., McManus, J. F., Berger, A., Brovkin, V., Kiefer, T. 2009. Interglacial diversity. Nature Geoscience 2(11), 751-755.

Ulbrich, U., Lionello, P., Belušić, D., Jacobeit, J., Knippertz, P., Kuglitsch, F. G., Ziv, B. 2012. Climate of the Mediterranean: synoptic patterns, temperature, precipitation, winds, and their extremes. In The Climate of the Mediterranean Region -From the Past to the Future. Elsevier.

Vogel, H., Wagner, B., Zanchetta, G., Sulpizio, R., Rosen, P. 2010. A paleoclimate record with tephrochronological age control for the last glacial-interglacial cycle from Lake Ohrid, Albania and Macedonia. Journal of Paleolimnology 44 (1), 295-310.

Wagner, B., Lotter, A. F., Nowaczyk, N., Reed, J. M., Schwalb, A., Sulpizio, R., Valsecchi, V., Wessels, M., and Zanchetta, G. 2009. A 40,000-year record of environmental change from ancient Lake Ohrid (Albania and Macedonia), Journal of Paleolimnology 41, 407–430.

Wagner B., Francke A., Sulpizio R., Zanchetta G., Lindhorst K., Krastel S., Vogel H., Rethemeyer J., Daut G., Grazhdani A., Lushaj B., Trajanovski S. 2012. Possible earthquake trigger for 6th century mass wasting deposit at Lake Ohrid (Macedonia/Albania). Climate of the Past 8, 2069-2078.

Wagner B., Wilke T., Francke A., Albrecht C., Baumgarten H., Bertini A., 4, Combourieu-Nebout N., Cvetkoska A., D´Addabbo M., Donders T.H., Föller K., Giaccio B., Grazhdani A., Hauffe T., Holtvoeth J., Joannin S., Jovanovska E., Just J., Kouli K., Koutsodendris A., Krastel S., Lacey J.H., LeicherN., Leng M.J., Levkov Z., Lindhorst K., Masi A., Mercuri A.M., Nomade S., Nowaczyk N., Panagiotopoulos K., Peyron O., Reed J.M., E. Regattieri E., Sadori L., Sagnotti L., Stelbrink B., Sulpizio R., Tofilovska S., Torri P., Vogel H., Wagner T., Wagner-Cremer F., Wolff G.A., Wonik T., Zanchetta G., Zhang X.S., 2017. The environmental and evolutionary history of Lake Ohrid (FYROM/Albania): Interim results from the SCOPSCO deep drilling project. Accepted, Biogeosciences. DOI: BG-2016-475

Wassenburg, J. A., Immenhauser, A., Richter, D. K., Jochum, K. P., Fietzke, J., Deininger, M., ... & Sabaoui, A. 2012. Climate and cave control on Pleistocene/Holocene calcite-to-aragonite transitions in speleothems from Morocco: elemental and isotopic evidence. Geochimica et Cosmochimica Acta 92, 23-47.

Watzin, M., Puka, V., and Naumoski, T. 2002. Lake Ohrid and its Watershed. State of the Environment Report, Lake Ohrid Conservation Project, Tirana, Albania and Ohrid, Macedonia.

Woodhead, J., Hellstrom, J., Maas, R., Drysdale, R., Zanchetta, G., Devine, P., Taylor, E. (2006). U–Pb geochronology of speleothems by MC-ICPMS. Quaternary Geochronology 1(3), 208-221.

Xoplaki, E., Gonzalez-Rouco, J. F., Luterbacher, J., Wanner, H. 2003. Mediterranean summer air temperature variability and its connection to the large-scale atmospheric circulation and SSTs. Climate Dynamics 20(7-8), 723-739.

Ye, Y., Smyth, J. R., Boni, P. 2012. Crystal structure and thermal expansion of aragonite-group carbonates by single-crystal X-ray diffraction. American Mineralogist 97(4), 707-712.

Yonge, C. J., Ford, D. C., Gray, J., Schwarcz, H. P. 1985. Stable isotope studies of cave seepage water. Chemical Geology: Isotope Geoscience section 58(1), 97-105.

Zanchetta, G., Drysdale, R.N., Hellstrom, J.C., Fallick, A.E., Isola, I., Gagan, M., Pareschi, M.T. 2007. Enhanced rainfall in the western Mediterranean during deposition of sapropel S1: stalagmite evidence from Corchia Cave (Central Italy). Quaternary Science Reviews 26, 279–286.

Zanchetta, G., Borghini, A., Fallick, A.E., 2007b. Late Quaternary palaeohydrology of Lake Pergusa (Sicily, southern Italy) as inferred by stable isotopes of lacustrine carbonates. Journal of Paleolimnology 38, 227–239.

Zanchetta, G., van Welden, A. Baneschi, I, et al. 2012. Multiproxy record for the last 4500 years from Lake Shkodra (Albania/ Montenegro). Journal of Quaternary Science 27, 780–789.

Zanchetta, G., Bar-Matthews, M., Drysdale, R. N., Lionello, P., Ayalon, A., Hellstrom, J. C., Isola, I., Regattieri, E. 2014. Coeval dry events in the central and eastern Mediterranean basin at 5.2 and 5.6 ka recorded in Corchia (Italy) and Soreq caves (Israel) speleothems. Global and Planetary Change 122, 130-139.

Zanchetta, G., Regattieri, E., Isola, I., Drysdale, R. N., Bini, M., Baneschi, I., Hellstrom, J. C. 2016a. The so-called “4.2 event” in the central Mediterranean and its climatic teleconnections. Alpine and Mediterranean Quaternary 29(2016), 5-17.

Zanchetta, G., Regattieri, E., Giaccio, B., Wagner, B., Sulpizio, R., Francke, A., Vogel, H., Sadori, L., Masi, A., Sinopoli, G., Lacey, J.H., Leng, M.L., Leicher, N. 2016b. Aligning MIS5 proxy records from Lake Ohrid (FYROM) with independently dated Mediterranean archives: implications for core chronology. Biogeosciences 13, 1-12.

Zhang, H., Cai, Y., Tan, L., Qin, S., An, Z. 2014. Stable isotope composition alteration produced by the aragonite-to-calcite transformation in speleothems and implications for paleoclimate reconstructions. Sedimentary Geology 309, 1-12.

Zhornyak, L.V., Zanchetta, G., Drysdale, R.N., Hellstrom, J.C., Isola, I., Regattieri, E., Piccini, L., Baneschi, I., Couchoud, I. 2011. Stratigraphic evidence for a “pluvial phase” between ca 8.2 and 7.1 ka from Renella Cave (Central Italy). Quaternary Science Reviews 30, 409–417.

Figures and Tables captions

Figure 1- Upper panel: location of Ohrid and of other sites mentioned in the text. Lower panel: Schematic geological map of the site and location of the cave entrance.

Figure 2: The stalagmite OH2

Figure 3: Age-depth models (thick darker lines), 95% confidence intervals (thin lighter lines) and ages for OH2. In blue the upper calcite section, in red the lower calcite and the aragonite portion; ages in light blue and red from the calcite, ages in green from the aragonite. Ages in yellow were removed as outlier (the left one) or for analytical problem (the right one).

Figure 4: A-E: Microphotographs of thin sections from stalagmite OH2 (A-D crossed nicols; E parallel nicols). The OH2 sketch (low-right corner) indicates the position of the microphotographs.

Figure 5: Temporal resolution (yr for mm of growth, A, obtained by calculating the age difference between each isotope point) and stable isotope results (B carbon; C oxygen) for stalagmite OH2. In grey original values for the aragonite (on both B and C) and in dark blue (on C) calcite-calibrated aragonite values (see text for details). Dotted lines indicate similar variations between oxygen and carbon records. The gray rectangle indicates the interval of anticorrelation between $\delta^{13}C$ and $\delta^{18}O$ values. The OH2 record is then compared with proxies time series from Lake Ohrid: D) TIC (Francke et al., 2016); E) $\delta^{18}O$ of lake endogenic calcite (Lacey et al., 2016); F) arboreal pollen percentage (excluding pinus, which is over-represented in the Ohrid record, Sadori et al., 2016b).

Figure 6: comparison of OH2 $\delta^{18}O$ record (A) with B) High resolution arboreal pollen record from Tenaghi Philippon (Fletcher et al., 2013); C) Pollen record (temperate pollen) from core MD01-2443 (Tzedakis et al., 2004; Roucoux et al., 2006); yellow dotted lines indicate the proposed correlations between wet period in the speleothem record and intervals of expansion of arboreal vegetation at Tenaghi. D) Uk 37 SST from core MD01-2443 (Roucoux et al., 2006, orange line; Martrat et al., 2004, brown line) and from core PRGL 1 (Cortina et al., 2015, red line). At the bottom, Marine Isotope Stages and Substages are also reported (from Railsback et al., 2015).

Table 1- Modal abundancies of calcite and aragonite as evaluated from the Rietveld study for the analyzed samples in the basal aragonitic interval of OH2.

Table 2: Corrected (in bold) and uncorrected U/Th ages for OH2 stalagmite. The activity ratios have been standardized to the HU-1 secular equilibrium standard, and ages calculated using decay constants of 9.195×10^{-6} (^{230}Th) and 2.835×10^{-6} (^{234}U). Depths are mm from top. Ages in italics were made on aragonite. Ages with asterisk were rejected as outliers. The double line represents the growth interruption.

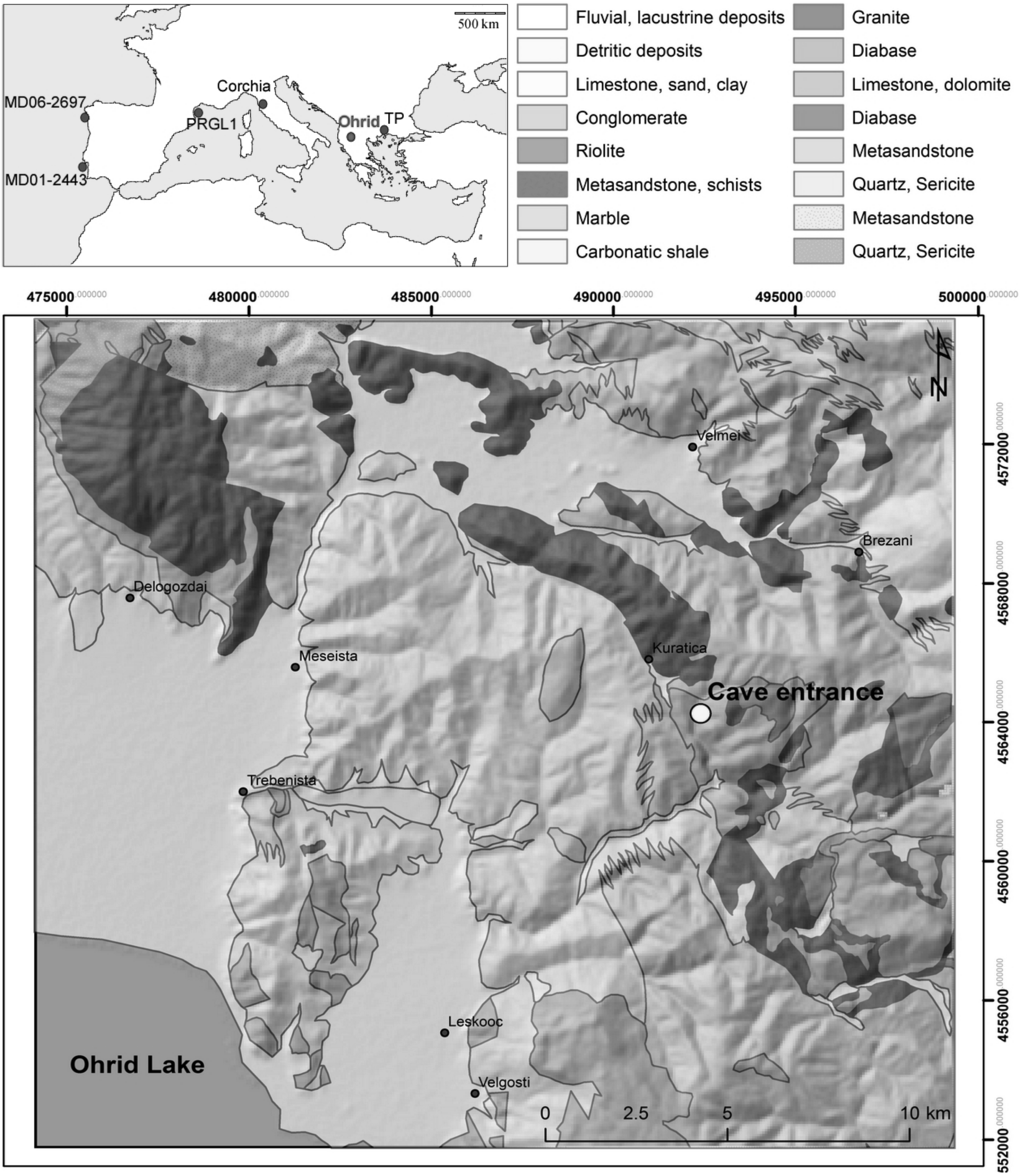
500 km
MD06-2697
MD01-2443
PRGL1
Corchia
Ohrid
TP
Fluvial, lacustrine deposits
Detritic deposits
Limestone, sand, clay
Conglomerate
Riolite
Metasandstone, schists
Marble
Carbonatic shale
Granite
Diabase
Limestone, dolomite
Diabase
Metasandstone
Quartz, Sericite
Metasandstone
Quartz, Sericite
475000
480000
485000
490000
495000
500000
4572000
4568000
4564000
4560000
4556000
4552000
Velmei
Brezani
Delogozdai
Meseista
Kuratica
Cave entrance
Trebenista
Leskooc
Velgosti
Ohrid Lake
0
2.5
5
10 km

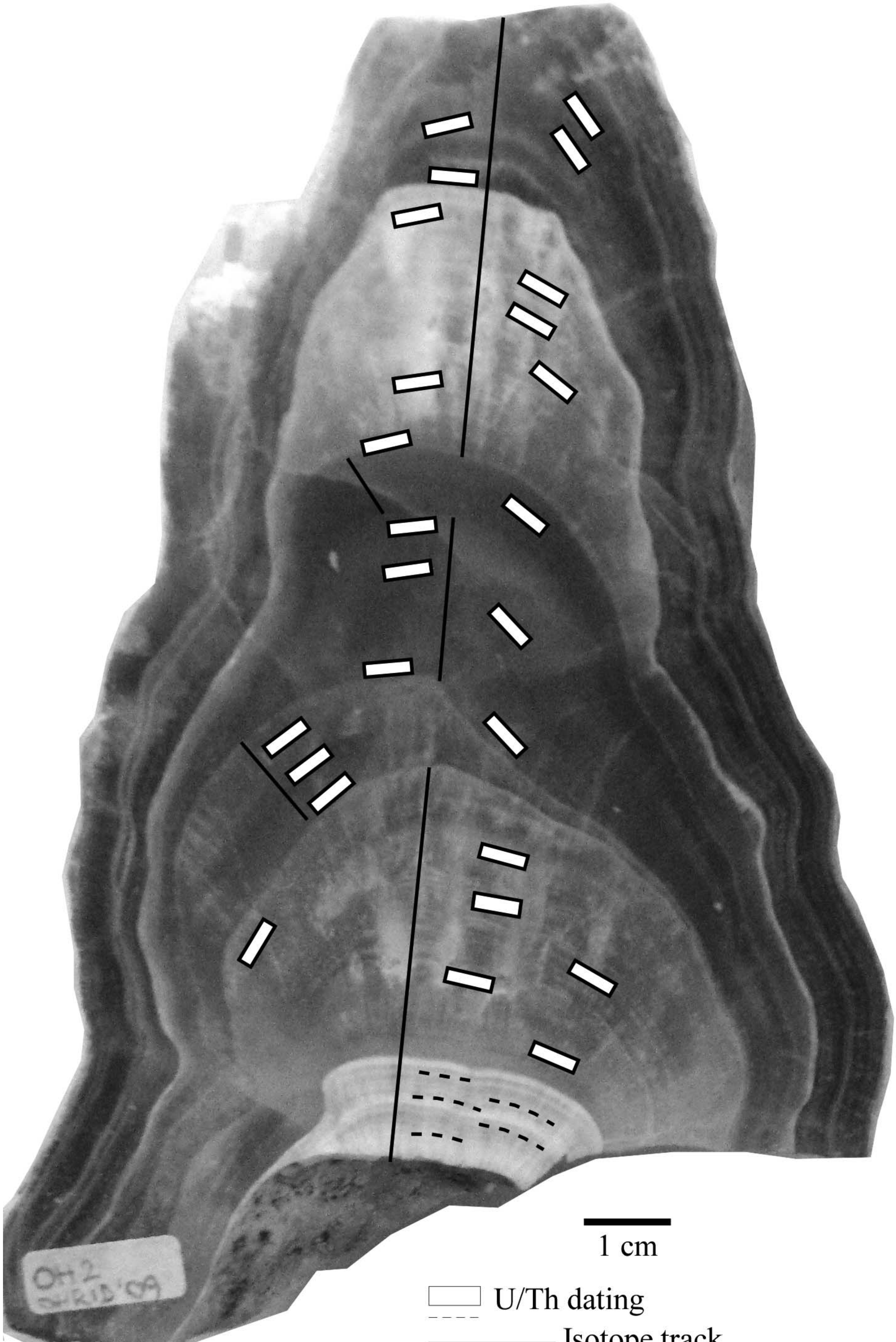

1 cm
U/Th dating
Isotope track

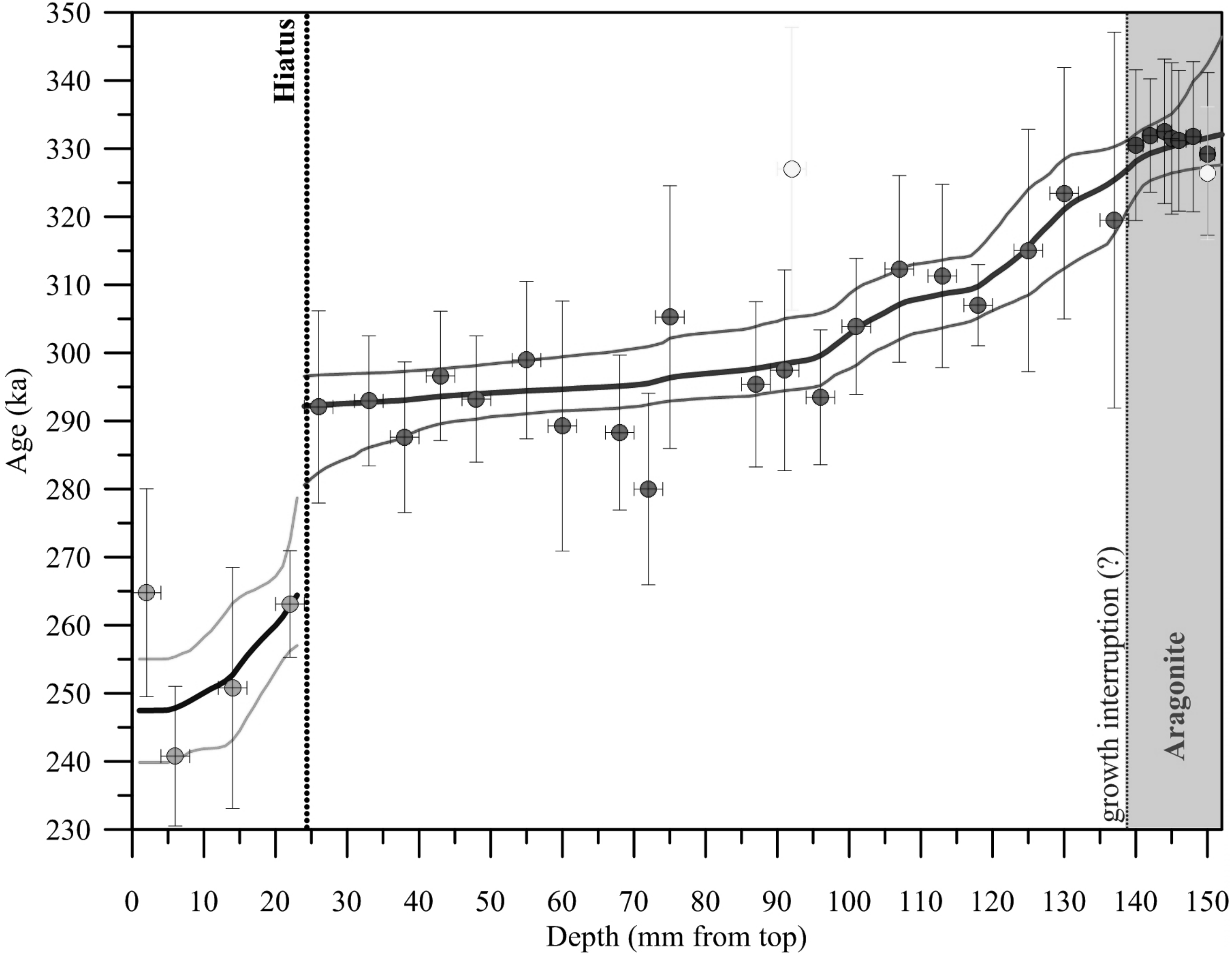

Hiatus
growth interruption (?)
Aragonite
Age (ka)
350
340
330
320
310
300
290
280
270
260
250
240
230
0
10
20
30
40
50
60
70
80
90
100
110
120
130
140
150
Depth (mm from top)

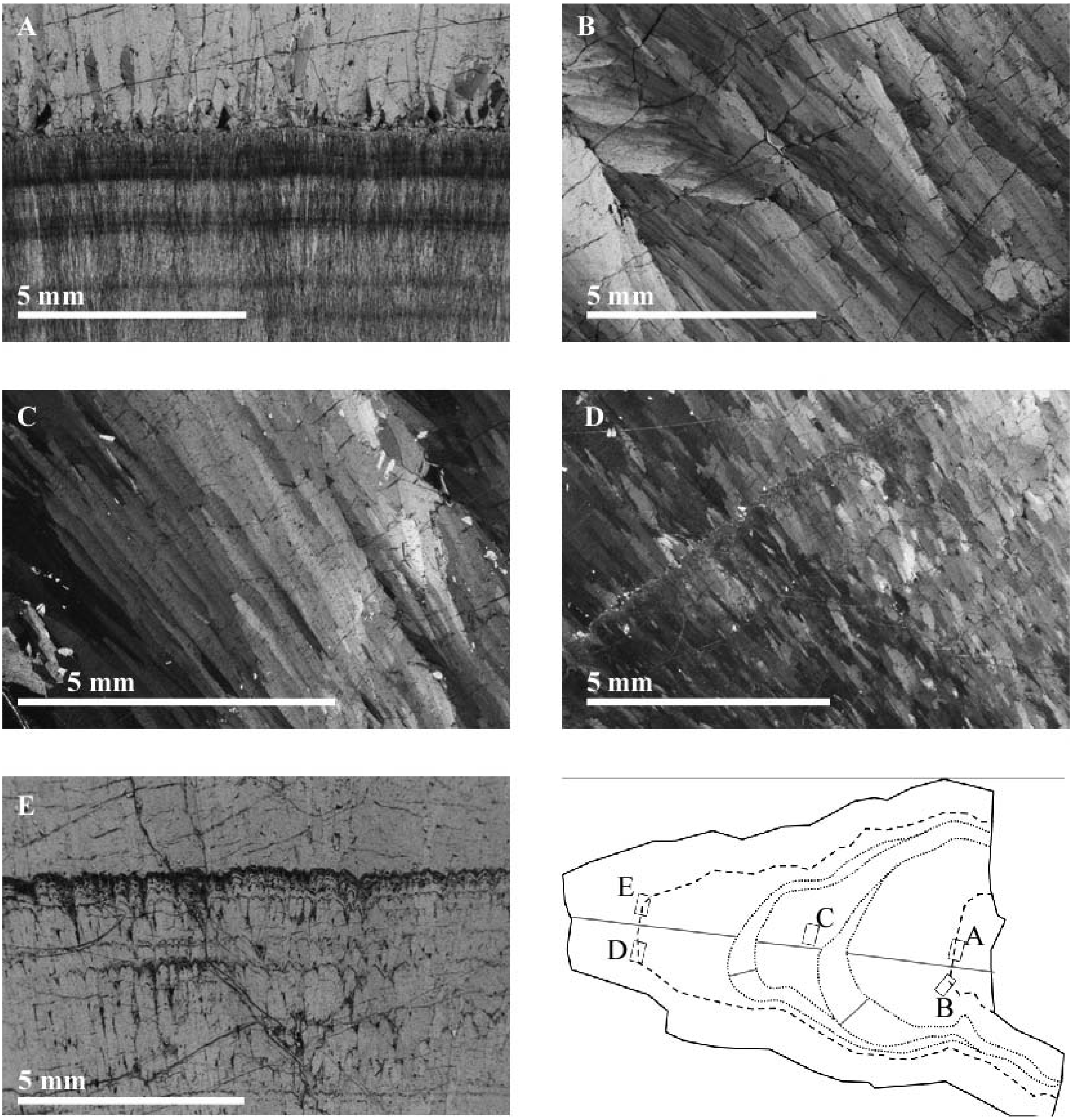
A
5 mm
B
5 mm
C
5 mm
D
5 mm
E
5 mm
E
D
C
A
B

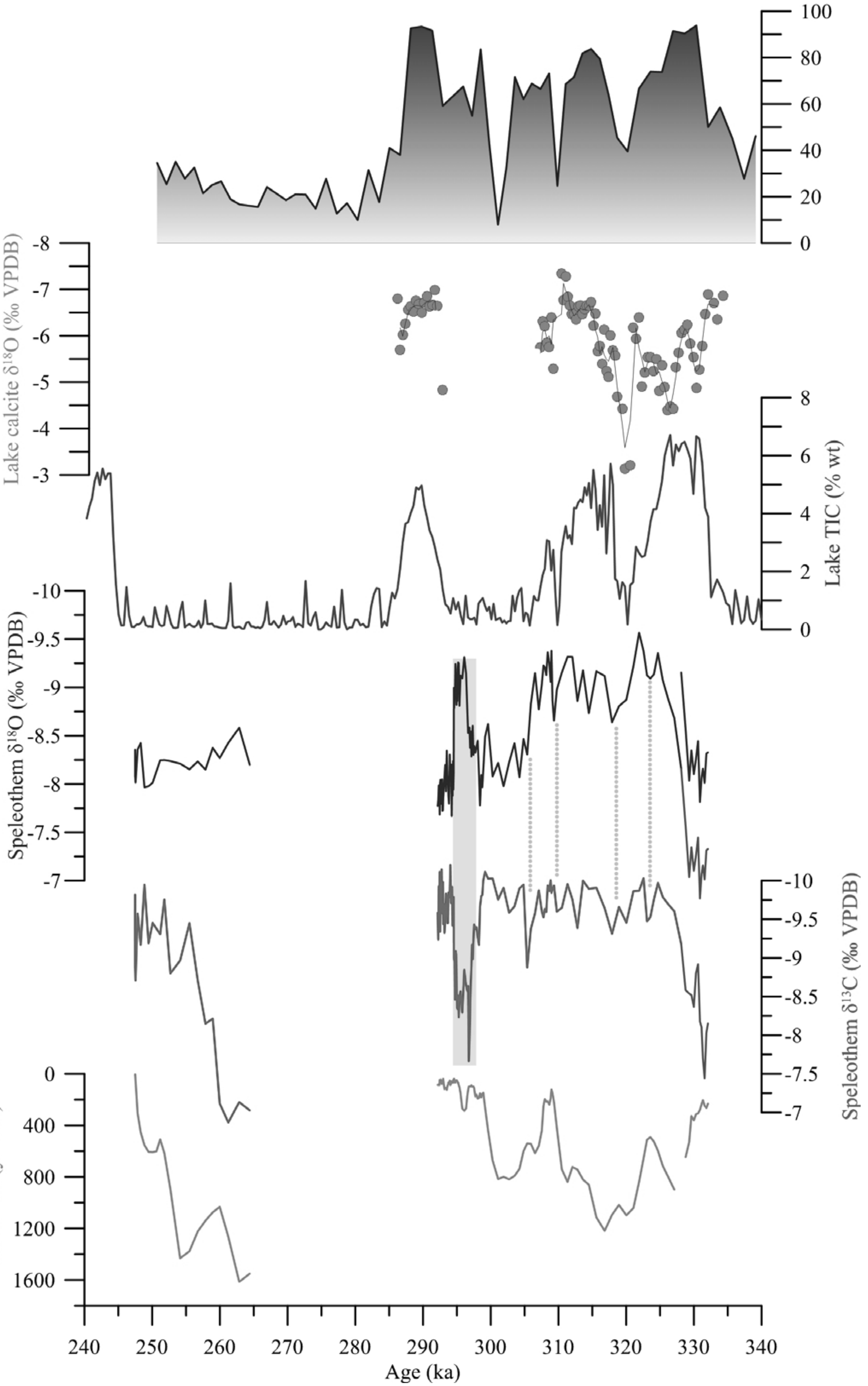

100
80
60
40
20
0
-8
-7
-6
-5
-4
-3
Lake calcite δ18O (‰ VPDB)
8
6
4
2
0
Lake TIC (% wt)
-10
-9.5
-9
-8.5
-8
-7.5
-7
Speleothem δ18O (‰ VPDB)
-10
-9.5
-9
-8.5
-8
-7.5
-7
Speleothem δ13C (‰ VPDB)
0
400
800
1200
1600
Resolution (yr/mm)
240
250
260
270
280
290
300
310
320
330
340
Age (ka)

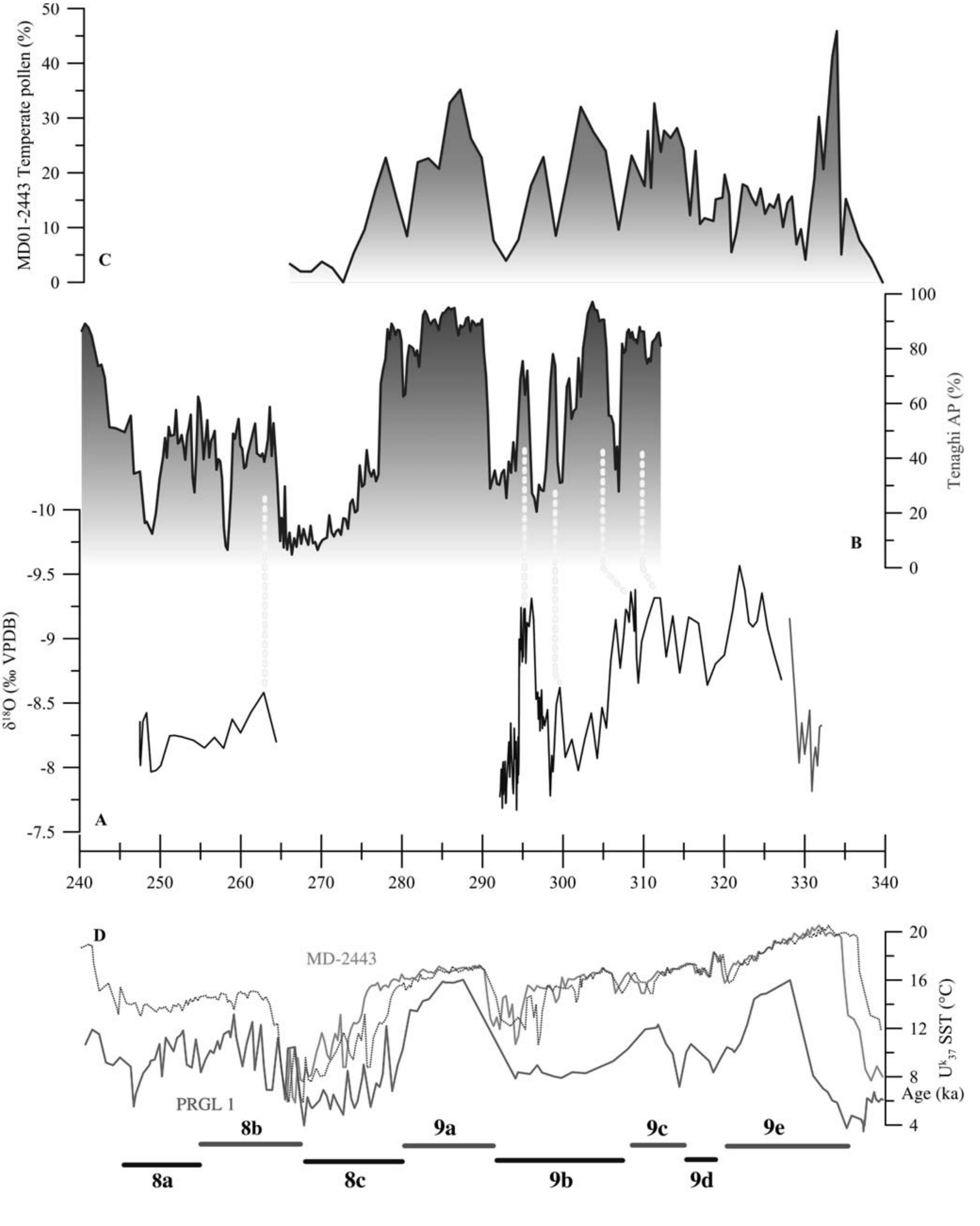

MD01-2443 Temperate pollen (%)
50
40
30
20
10
0
C
Tenaghi AP (%)
100
80
60
40
20
0
B
δ18O (‰ VPDB)
-10
-9.5
-9
-8.5
-8
-7.5
A
240
250
260
270
280
290
300
310
320
330
340
D
MD-2443
PRGL 1
Uk37 SST (°C)
20
16
12
8
4
Age (ka)
8a
8b
8c
9a
9b
9c
9d
9e

Sample name	depth	aragonite (%)	calcite (%)
OH2 C	143	12.6	87.4
OH2 B	147	4.3	95.7
OH2 A	151	5.7	94.3

Table 1

Sample ID	^{238}U ng/g	depth	$^{230}Th/^{238}U$	$^{234}U/^{238}U$	Age uncr (ka)	$^{232}Th/^{238}U$	$^{230}Th/^{232}Th$	**Age cr Ka**	***2se(ka)***
OH2-3	76	2.00	1.1749	1.2217	267.136	0.021144	55.6	**264.771**	**15.279**
OH2-6	63	6.00	1.0816	1.1632	246.155	0.042439	25.5	**240.769**	**10.243**
OH2-14	38	14.00	1.1189	1.1779	263.126	0.095959	11.7	**250.793**	**17.697**
OH2 C	29	22.00	1.1787	1.2279	264.017	0.008066	146.1	**263.112**	**7.829**
OH2-24	95	26.00	1.2466	1.2589	292.140	0.000612	2035.5	**292.050**	**14.113**
OH2-31	113	33.00	1.2162	1.2332	292.935	0.000310	3929.4	**292.940**	**9.552**
OH2-38	111	38.00	1.2040	1.2275	287.586	0.000255	4715.2	**287.615**	**11.063**
OH2-41	105	43.00	1.2072	1.2230	296.655	0.000532	2267.5	**296.618**	**9.499**
OH2-48	84	48.00	1.2083	1.2265	293.220	0.000524	2305.2	**293.211**	**9.275**
OH2-B	96	55.00	1.2188	1.2309	297.656	0.000216	5631.5	**298.935**	**11.557**
OH2-59	35	60.00	1.2900	1.2908	296.633	0.071792	18.0	**289.258**	**18.360**
OH2-66	33	68.00	1.2313	1.2491	288.703	0.003664	336.1	**288.302**	**11.376**
OH2-72	40	72.00	1.2437	1.2668	280.365	0.003505	354.8	**279.999**	**14.068**
OH2-74	41	75.00	1.3534	1.3351	305.576	0.003709	364.9	**305.245**	**19.289**
OH2-84	44	87.00	1.2176	1.2309	297.479	0.019795	61.5	**295.390**	**12.138**
OH2-92	54	91.00	1.2687	1.2721	298.133	0.007243	175.2	**297.441**	**14.736**
OH2-94*	42	92.00	1.2899	1.2689	327.496	0.004670	276.2	**327.027***	**20.795**
OH2-93	62	96.00	1.2233	1.2384	293.757	0.002637	463.8	**293.463**	**9.903**
OH2 D	47	101.00	1.2271	1.2339	303.850	0.000141	8681.3	**303.890**	**9.986**
OH2-100	99	107.00	1.2150	1.2185	312.365	0.000446	2722.2	**312.329**	**13.706**
OH2-107	104	113.00	1.2099	1.2151	311.316	0.000398	3037.7	**311.287**	**13.454**
OH2-103	100	118.00	1.1897	1.2015	306.998	0.000140	8526.9	**307.004**	**5.964**
OH2-123	95	125.00	1.2218	1.2223	315.128	0.001263	967.4	**315.027**	**17.787**
OH2-124	79	130.00	1.1345	1.1479	323.557	0.001260	900.5	**323.423**	**18.463**
OH2-A	61	137.00	1.1351	1.1510	317.150	0.001244	912.6	**319.500**	**27.601**
OH2-135	*11539*	*140.00*	*1.1989*	*1.1951*	*330.527*	*0.000133*	*8985.4*	***330.500***	***11.060***
OH2-132	*4785*	*142.00*	*1.2217*	*1.2123*	*331.944*	*0.000076*	*15971.2*	***331.908***	***8.326***
OH2-137	*9585*	*144.00*	*1.1982*	*1.1935*	*332.485*	*0.000008*	*152603.4*	***332.521***	***10.611***
OH2-138	*11589*	*145.00*	*1.1946*	*1.1912*	*331.515*	*0.000017*	*72226.1*	***331.475***	***11.117***
OH2-140	*10516*	*146.00*	*1.2162*	*1.2084*	*331.172*	*0.000038*	*31710.0*	***331.161***	***10.344***
OH2-142	*14646*	*148.00*	*1.2120*	*1.2048*	*331.731*	*0.000017*	*72426.6*	***331.752***	***11.027***
OH2-145	*4424*	*150.00*	*1.2060*	*1.2014*	*329.200*	*0.000049*	*24721.5*	***329.228***	***11.928***
*OH2-145**	*1943*	*150.00*	*1.2047*	*1.2019*	*326.326*	*0.000047*	*25810.4*	***326.368****	***9.783***

Table 2

OH-2A

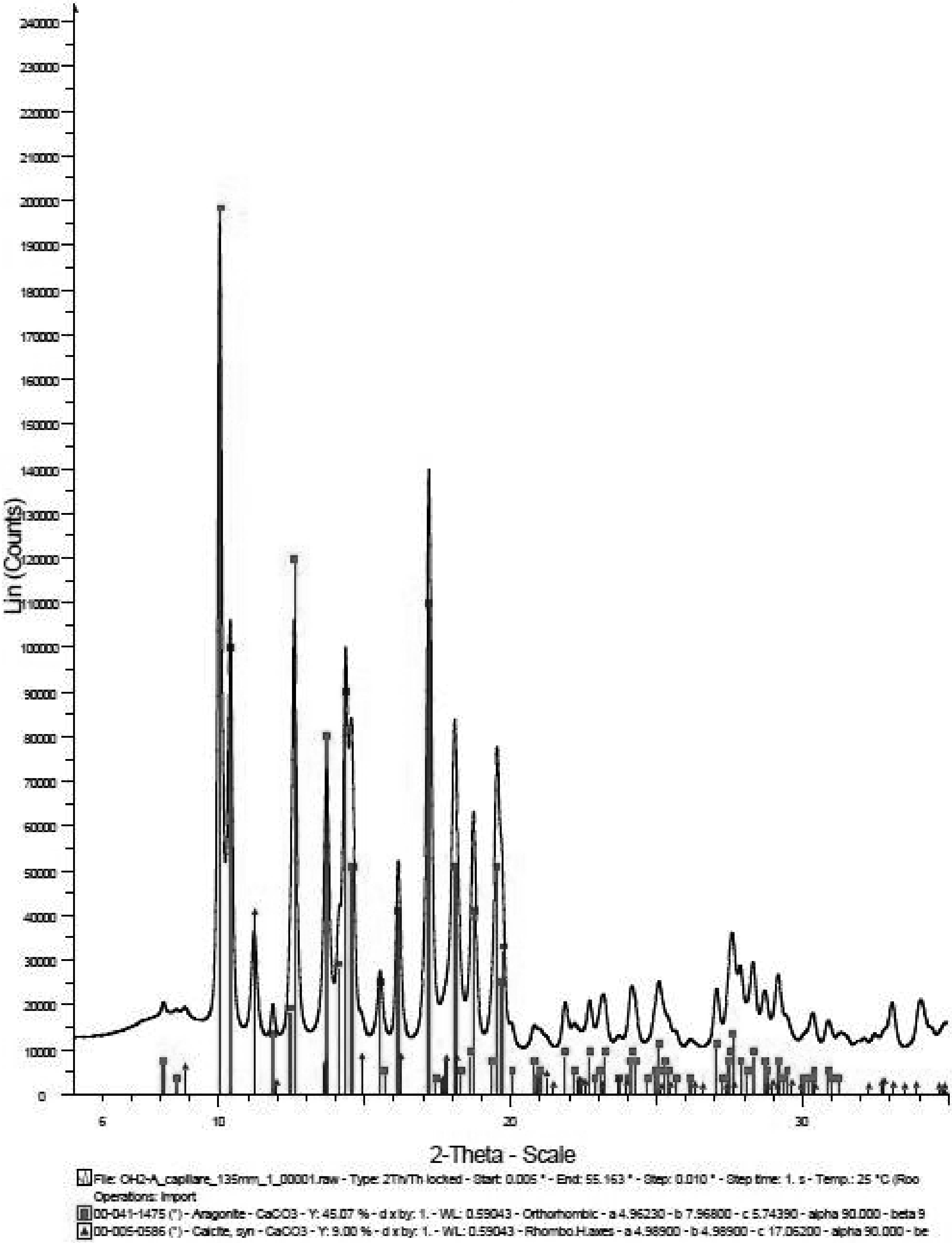

Lin (Counts)
240000
230000
220000
210000
200000
190000
180000
170000
160000
150000
140000
130000
120000
110000
100000
90000
80000
70000
60000
50000
40000
30000
20000
10000
0
6
10
20
30
2-Theta - Scale
File: OH2-A_capillare_135mm_1_00001.raw - Type: 2Th/Th locked - Start: 0.005 ° - End: 55.163 ° - Step: 0.010 ° - Step time: 1. s - Temp.: 25 °C (Roo
Operations: Import
00-041-1475 (*) - Aragonite - CaCO3 - Y: 45.07 % - d x by: 1. - WL: 0.59043 - Orthorhombic - a 4.96230 - b 7.96800 - c 5.74390 - alpha 90.000 - beta 9
00-005-0586 (*) - Calcite, syn - CaCO3 - Y: 9.00 % - d x by: 1. - WL: 0.59043 - Rhombo.H.axes - a 4.98900 - b 4.98900 - c 17.06200 - alpha 90.000 - be

OH-2B

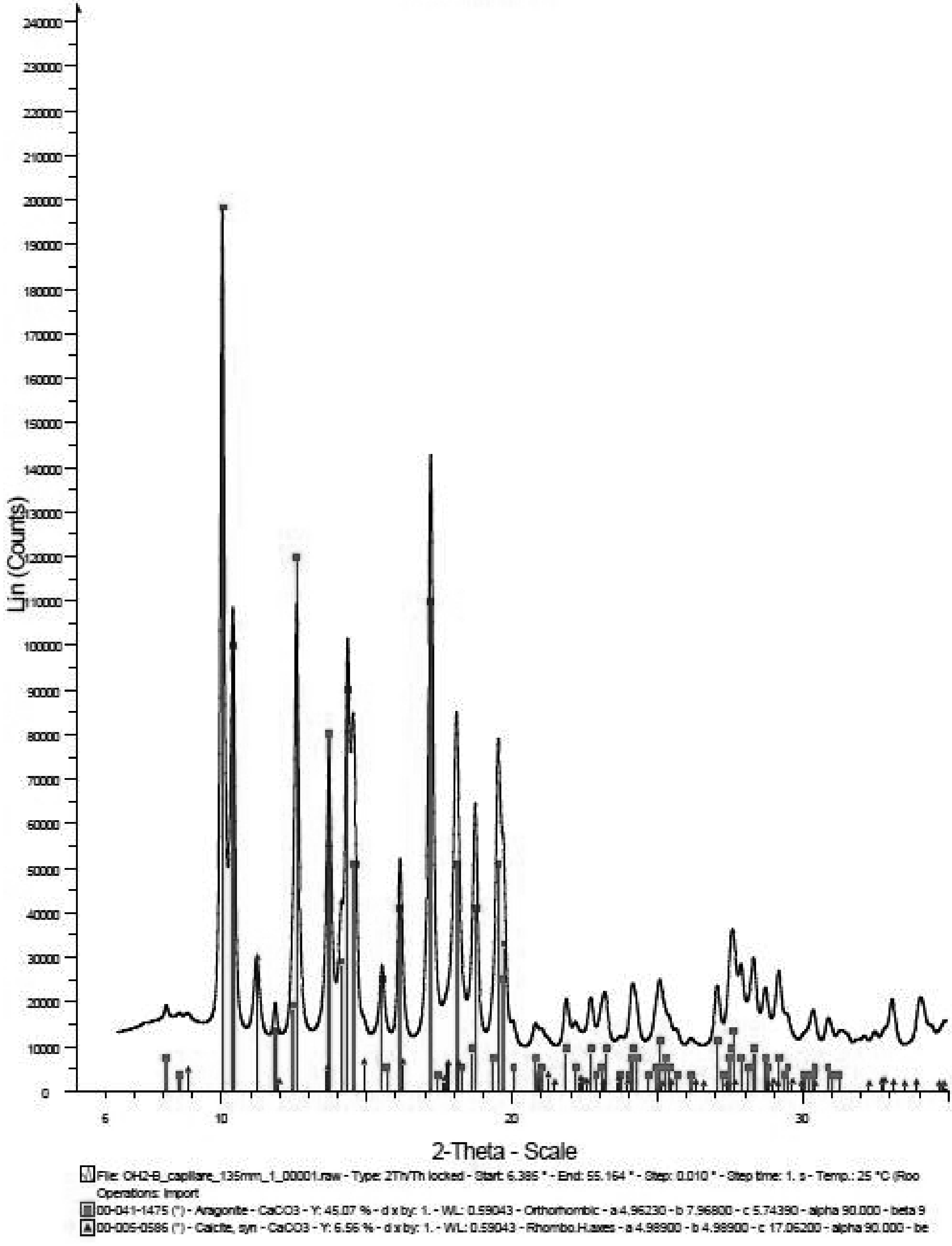

Lin (Counts)
0
10000
20000
30000
40000
50000
60000
70000
80000
90000
100000
110000
120000
130000
140000
150000
160000
170000
180000
190000
200000
210000
220000
230000
240000
6
10
20
30
2-Theta - Scale
File: OH2-B_capillare_135mm_1_00001.raw - Type: 2Th/Th locked - Start: 6.385 ° - End: 55.164 ° - Step: 0.010 ° - Step time: 1. s - Temp.: 25 °C (Roo
Operations: Import
00-041-1475 (*) - Aragonite - CaCO3 - Y: 45.07 % - d x by: 1. - WL: 0.59043 - Orthorhombic - a 4.96230 - b 7.96800 - c 5.74390 - alpha 90.000 - beta 9
00-005-0586 (*) - Calcite, syn - CaCO3 - Y: 6.56 % - d x by: 1. - WL: 0.59043 - Rhombo.H.axes - a 4.98900 - b 4.98900 - c 17.06200 - alpha 90.000 - be

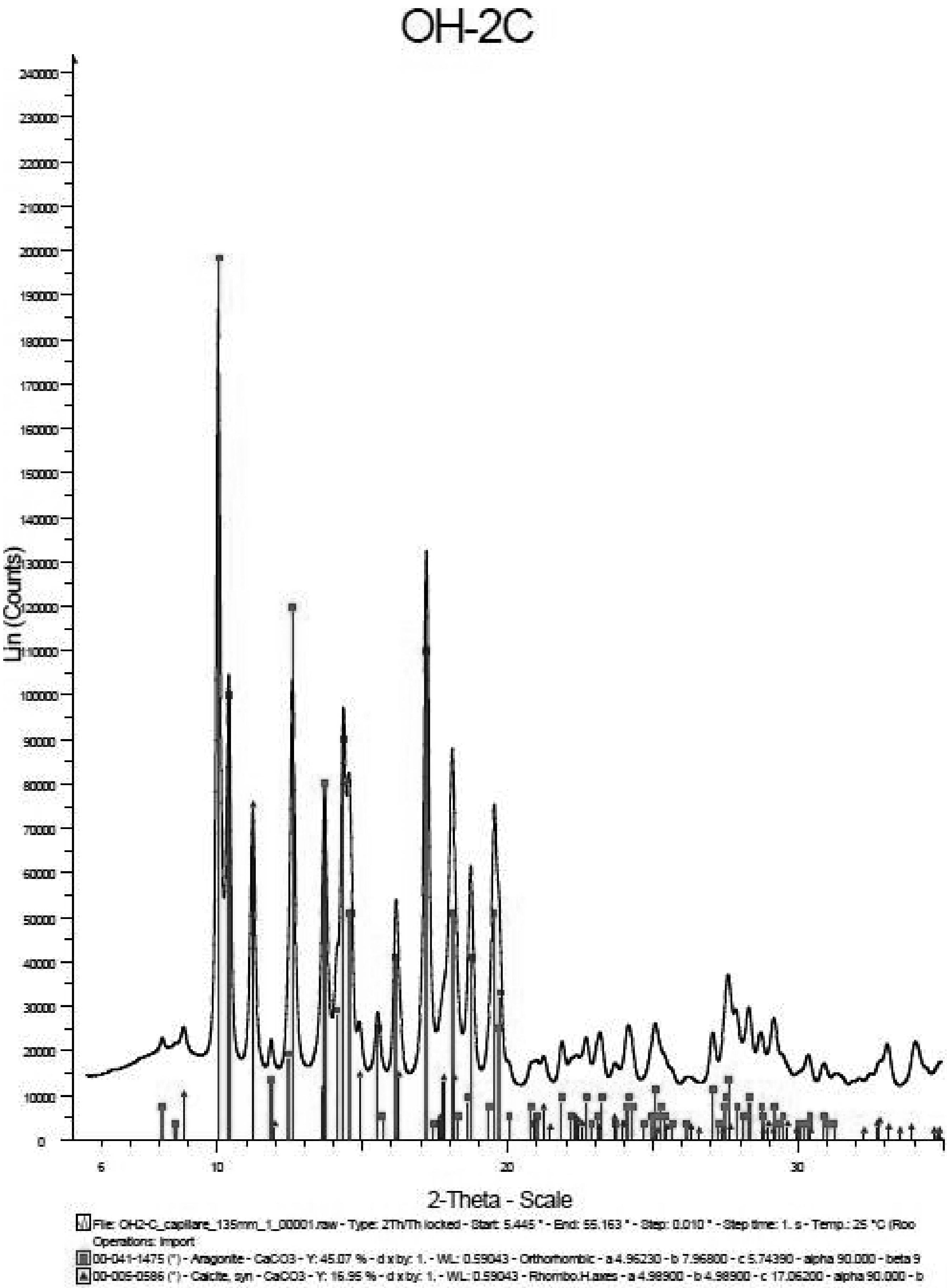
OH-2C
Lin (Counts)
0
10000
20000
30000
40000
50000
60000
70000
80000
90000
100000
110000
120000
130000
140000
150000
160000
170000
180000
190000
200000
210000
220000
230000
240000
6
10
20
30
2-Theta - Scale
File: OH2-C_capillare_135mm_1_00001.raw - Type: 2Th/Th locked - Start: 5.445 ° - End: 55.163 ° - Step: 0.010 ° - Step time: 1. s - Temp.: 25 °C (Roo
Operations: Import
00-041-1475 (*) - Aragonite - CaCO3 - Y: 45.07 % - d x by: 1. - WL: 0.59043 - Orthorhombic - a 4.96230 - b 7.96800 - c 5.74390 - alpha 90.000 - beta 9
00-005-0586 (*) - Calcite, syn - CaCO3 - Y: 16.95 % - d x by: 1. - WL: 0.59043 - Rhombo.H.axes - a 4.98900 - b 4.98900 - c 17.06200 - alpha 90.000 - b

sample	*Rp* (%)	*Rwp* (%)	*GoF*
OH2-A	6.696	9.061	13.721
OH2-B	7.063	9.465	14.199
OH2-C	5.907	7.995	12.727

Table S1- Agreement factors for Rietveld refinement.

Calcite	*a*	*c*	d_{104}
OH2-A	4.983(3)	17.07(1)	3.035
OH2-B	4.990(4)	17.06(1)	3.036
OH2-C	4.984(1)	17.049(5)	3.032
Effenberger et al	4.9896(2)	17.061(1)	3.035

Table S2- Refined cell parameters for calcite.

	a Mg_{mol}	c Mg_{mol}	d_{104} Mg_{mol}
OH2-A	1.5	0	0
OH2-B	0	0	0
OH2-C	1.5	0	0

Table S3- Mg content in calcite, evaluated according to Zhang *et al.* (2010).

Aragonite	*a*	*b*	*c*
OH2-A	4.9533(3)	7.9816(6)	5.7404(4)
OH2-B	4.9541(3)	7.9805(6)	5.7407(4)
OH2-C	4.9528(3)	7.9821(6)	5.7409(4)
Ye *et al.*(2012)	4.9596(5)	7.9644(7)	5.7416(5)

Table S4- Refined cell parameters for aragonite.